

Charting the Flavour Structure of Dark Matter

Simone Biondini,^{1,*} Admir Greljo,^{2,†} Xavier Ponce Díaz,^{2,‡} and Alessandro Valenti^{2,§}

¹*Institute of Physics, University of Freiburg, Hermann-Herder-Straße 3, 79014 Freiburg, Germany*

²*Department of Physics, University of Basel, Klingelbergstrasse 82, CH-4056 Basel, Switzerland*

What flavour structure of t -channel thermal dark matter remains compatible with current flavour physics and direct detection bounds? We broadly chart the space of hypotheses using the framework of flavour symmetries and their breaking patterns. We then focus on scenarios in which the fermionic dark matter and its scalar mediator are flavour singlets, falling into the class of *rank-1 flavour violation*. For two representative benchmarks, quarkphilic (q_L) and leptophilic (e_R), we perform a comprehensive phenomenological analysis, fitting the relic abundance and examining the interplay among flavour observables, direct detection, and collider searches. Our results quantify the allowed deviations from flavour-symmetric limits and assess the discovery prospects in future flavour and direct detection experiments.

Contents

1. Introduction	1
2. Charting Dark Matter with Flavour Symmetries	2
2.1. Minimal Flavour Violation	2
2.2. $U(2)^5$ flavour symmetry	3
2.3. Minimal Flavour Protection	4
3. Leptophilic Dark Matter	6
3.1. Relic Abundance	7
3.2. Direct (and Indirect) Detection	8
3.3. Collider Searches	8
3.4. Flavour Observables	9
3.5. Interplay and Summary	9
3.5.1. Majorana Dark Matter	10
3.5.2. Dirac Dark Matter	12
4. Quarkphilic Dark Matter	12
4.1. Relic Abundance	13
4.2. Collider Searches	14
4.3. Direct (and Indirect) Detection	14
4.4. Flavour Observables	15
4.5. Interplay and Summary	16
4.5.1. Majorana Dark Matter	16
4.5.2. Dirac Dark Matter	17
5. Conclusion	18
A. SMEFT Matching and Flavour Observables	19
A1. Matching to the SMEFT	19
A2. Flavour Observables	20
B. Flavour Reparametrization	22
C. Cross sections for dark matter freeze-out	23
References	24

1. Introduction

The freeze-out mechanism remains one of the most compelling paradigms explaining the observed abundance of dark matter (DM) as a thermal relic [1–3]. Through its interactions with the Standard Model (SM), DM is initially in thermal equilibrium with the primordial plasma; as the temperature falls below its mass, the equilibrium density becomes exponentially suppressed, and annihilations can no longer keep pace with the Hubble expansion, leading to freeze-out. Remarkably, particles with masses around the TeV scale and $\mathcal{O}(1)$ couplings with the SM naturally reproduce the observed DM relic density, a coincidence often referred to as *the WIMP miracle*. This observation hints at a deep connection between cosmology and the energy frontier of particle physics, possibly suggesting a common origin of the electroweak scale and DM.

Despite decades of null results from direct and indirect detection, as well as collider searches [4–6], these efforts continue to motivate a thorough and systematic exploration of the thermal dark matter parameter space, including well-motivated departures from the minimal WIMP paradigm [7, 8]. Such simplified models extend the SM by at least a dark matter candidate and a mediator. They can be broadly classified into two categories [9]: *t-channel models*, featuring renormalizable DM–mediator–SM interactions [10–18], and *s-channel models*, in which the mediator couples linearly to SM fields [19–26]. In this work, we consider *t*-channel models, which are particularly interesting from a flavour physics perspective.

Indeed, among complementary probes, thermal DM scenarios are directly tested by flavour physics [27–36]. TeV-scale new physics (NP) with $\mathcal{O}(1)$ couplings to SM particles must exhibit a highly non-trivial flavour structure to evade stringent bounds from flavour-changing neutral currents and CP-violating observables. This general fact is commonly referred to as the *new physics flavour puzzle* [37–41]. The same concerns, therefore, apply to DM interactions with the SM, motivating the central question of this work: what is the flavour structure of *t*-channel DM that remains compatible with existing bounds?

Flavour symmetries and their breaking patterns provide a robust framework for addressing this question in a structured and systematic manner. Build-

* simone.biondini@physik.uni-freiburg.de

† admir.greljo@unibas.ch

‡ xavier.poncediaz@unibas.ch

§ alessandro.valenti@unibas.ch

ing on recent applications of this approach to the SMEFT [42–46], we extend it to t -channel DM interactions. In Section 2, we chart the corresponding space of hypotheses by classifying the fields and couplings, formally treated as spurions, under a set of assumed flavour symmetries. Our work generalises the well-known case of Minimal Flavour Violation [47–50] and its variants [51–54]. Guided by general lessons from the SMEFT, we identify particularly well-motivated candidate scenarios for dedicated studies. For the other class of simplified DM models, namely s -channel scenarios, only the mediator couples directly to the SM fields. As a result, the flavour structure reduces to identifying the flavour representations of linear extensions of the SM [55] and their allowed couplings [56, 57], with the DM field itself playing no active role in flavour observables.

In the central part of this work, we test the flavour symmetry expectations on specific cases. For concreteness, we focus on the simplest benchmark scenarios in which both the DM particle and the mediator are flavour singlets. In this setup, the DM–mediator–SM coupling is a priori an arbitrary vector in the flavour space of the corresponding SM fermion, giving rise to *rank-1* flavour violation, for which we adopt the general parametrization introduced in recent B -physics studies [58, 59]. We perform a thorough phenomenological study of a leptophilic benchmark in Section 3 and a quarkphilic benchmark in Section 4. In each case, we compute the complete set of relevant flavour observables and confront them with the relic density requirement and complementary constraints from collider searches and direct detection (DD). This allows us to quantitatively assess whether, and to what extent, viable scenarios must lie close to flavour-symmetric limits, which is often assumed rather than tested in the existing literature. We conclude in Section 5 with a discussion of how these lessons generalize beyond the simplest scenarios.

2. Charting Dark Matter with Flavour Symmetries

The generic t -channel interaction between a SM fermion f_{SM} and the dark sector fields χ and Φ can be written as

$$\mathcal{L} \supset y \bar{f}_{\text{SM}} \chi \Phi + \text{h.c.} \quad (1)$$

Here we have suppressed flavour indices in both the fields and the coupling y . The fields χ and Φ are assumed to be odd under a stabilizing \mathcal{Z}_2 symmetry.¹ For the purposes of this section, it is not relevant whether the actual DM particle is either χ or Φ , which we will collectively denote by $X \equiv (\chi\Phi)$. Our focus is instead on the following question: what flavour structure of the coupling y allows the dark sector to

reproduce the observed DM relic abundance, while remaining compatible with constraints from flavour physics?

This question is particularly relevant for the t -channel models considered here. These scenarios favor dark sector masses in the range 0.1–10 TeV with $\mathcal{O}(1)$ couplings to achieve the observed relic abundance (see [10] for a recent review). On the other hand, precision measurements of flavour transitions among SM fermions are well known to constrain generic NP with $\mathcal{O}(1)$ flavour-violating couplings up to scales of $\mathcal{O}(\text{PeV})$ or higher [41]. Flavour-changing neutral currents (FCNC) are highly suppressed in the SM due to the non-generic structure of the Yukawa interactions, which gives rise to approximate flavour symmetries. In the quark sector, flavour violation is entirely controlled by the CKM matrix through weak interactions, leading, for example, to strong suppressions of FCNC via the GIM mechanism [61]. In the lepton sector, charged lepton flavour violation is suppressed by the smallness of neutrino masses through an analogous mechanism. NP can violate these approximate flavour symmetries and generate large flavour-violating effects, making FCNC exceptionally sensitive probes of physics beyond the SM.

The challenge of accommodating TeV-scale NP while satisfying flavour constraints is a general one. It is particularly well known in the context of solutions to the SM hierarchy problem, where new states near the TeV scale are required to stabilize the Higgs mass, but would generically introduce large sources of flavour violation, for a recent example, see [62]. To address this tension, the framework of flavour symmetries was introduced to organize new physics (NP) couplings in a controlled manner, meaning that the resulting flavour structure is stable under renormalization group evolution and does not rely on fine-tuned cancellations. This allows NP at much lower scales than in flavour-anarchic scenarios. Our goal is to adapt these tools to the present context and develop a systematic classification of t -channel DM models that reconciles the relic abundance requirement with stringent constraints from FCNC and CP violation. The presentation is intentionally pedagogical to remain accessible to readers not accustomed to the use of flavour symmetries in BSM model building.

2.1. Minimal Flavour Violation

When dealing with DM simplified models, the most widely studied framework in this context is Minimal Flavour Violation (MFV) [47–50, 63]. In MFV, the SM fields are assigned to the fundamental representations of the approximate flavour symmetry $U(3)^5$ respected by the gauge interactions, $f_{\text{SM}} \sim \mathbf{3}_f$. This symmetry is broken by the dimension four Yukawa interactions, leaving only the subgroup $U(1)_B \times U(1)_e \times U(1)_\mu \times U(1)_\tau$ unbroken. Importantly, this breaking pattern leads to the special suppression properties of flavour violation discussed above. New interactions such as the one in Eq. (1) would generically spoil this structure and thus lead to very strong flavour con-

¹ DM stability can be a consequence of unbroken discrete subgroups of flavour symmetries, see e.g. [48, 60].

straints.

The impact of NP on flavour can be elegantly understood by treating the couplings that break $U(3)^5$, namely the SM Yukawas and the new coupling y , as *spurions*. These are non-dynamical fields that transform under $U(3)^5$ in such a way that the full flavour symmetry is formally restored, and are then assigned fixed background values. In this language, NP couplings can avoid inducing large flavour violation in two ways. They may transform as flavour singlets, in which case they introduce no new sources of flavour breaking and can naturally be of order one. Alternatively, they may be constructed as product expansions in terms of the SM spurions, which in MFV are the Yukawa matrices themselves. In this case, flavour violation induced by NP is aligned with that of the SM and appears only as a small correction, allowing TeV-scale NP to remain compatible with current data.

Such an expansion is not always possible. The representation of the spurion y under $U(3)^5$ is fixed by the representations of f_{SM} and the dark sector operator X , since the product of all three must contain a singlet in order for the Lagrangian to be flavour invariant. An expansion of y in terms of the SM spurions,

$$Y_u \sim (\mathbf{3}_q, \bar{\mathbf{3}}_u), \quad Y_d \sim (\mathbf{3}_q, \bar{\mathbf{3}}_d), \quad Y_e \sim (\mathbf{3}_\ell, \bar{\mathbf{3}}_e), \quad (2)$$

is possible only if the representation of y appears in the decomposition of products of these spurions. When this condition is not satisfied, the breaking of $U(3)^5$ induced by y is not necessarily aligned with the SM one, and large new sources of flavour violation may be expected.

To make this discussion concrete, we present in Table I several examples of the representation of y under $U(3)^3$, the flavour group of the quark sector, as fixed by the interaction in Eq. (1) once the representations of f_{SM} and X are specified. In the table, entries shown in green correspond to representations that are either singlets under $U(3)^5$ or can be expanded purely in terms of Y_u . In these cases, the coupling y can naturally be of order one, supported by the large top Yukawa coupling, and TeV-scale dark sector masses can reproduce the observed relic abundance. Entries shown in yellow correspond to representations that can be expanded in terms of SM Yukawas but require at least one insertion of Y_d or Y_e . This implies an additional suppression by at least one power of $y_{b,\tau} \sim 10^{-2}$, which is too small to account for the relic abundance in most of the parameter space. Finally, uncolored entries correspond to representations that cannot be constructed from SM spurions.

2.2. $U(2)^5$ flavour symmetry

By enforcing flavour universality, the MFV expansion is often too restrictive, excluding phenomenologically viable and theoretically motivated possibilities. This is particularly evident in flavour-conserving processes involving light quarks, where bounds on NP are far stronger than in the heavy-flavour sector. Relevant to our study, DD bounds are highly stringent for DM

$X \setminus \bar{f}_{\text{SM}}$	$\bar{\mathbf{3}}_q$	$\bar{\mathbf{3}}_u$	$\bar{\mathbf{3}}_d$	$\bar{\mathbf{3}}_\ell$	$\bar{\mathbf{3}}_e$
$\mathbf{1}$	$\mathbf{3}_q$	$\mathbf{3}_u$	$\mathbf{3}_d$	$\mathbf{3}_\ell$	$\mathbf{3}_e$
$\mathbf{3}_q$	$\mathbf{1} \oplus \mathbf{8}_q$	$(\mathbf{3}_u, \bar{\mathbf{3}}_q)$	$(\mathbf{3}_d, \bar{\mathbf{3}}_q)$	$(\mathbf{3}_\ell, \bar{\mathbf{3}}_q)$	$(\mathbf{3}_e, \bar{\mathbf{3}}_q)$
$\bar{\mathbf{3}}_q$	$\bar{\mathbf{3}}_q \oplus \mathbf{6}_q$	$(\mathbf{3}_u, \mathbf{3}_q)$	$(\mathbf{3}_d, \mathbf{3}_q)$	$(\mathbf{3}_\ell, \mathbf{3}_q)$	$(\mathbf{3}_e, \mathbf{3}_q)$
$\mathbf{3}_u$	$(\mathbf{3}_q, \bar{\mathbf{3}}_u)$	$\mathbf{1} \oplus \mathbf{8}_u$	$(\mathbf{3}_d, \bar{\mathbf{3}}_u)$	$(\mathbf{3}_\ell, \bar{\mathbf{3}}_u)$	$(\mathbf{3}_e, \bar{\mathbf{3}}_u)$
$\bar{\mathbf{3}}_u$	$(\mathbf{3}_q, \mathbf{3}_u)$	$\bar{\mathbf{3}}_u \oplus \mathbf{6}_u$	$(\mathbf{3}_d, \mathbf{3}_u)$	$(\mathbf{3}_\ell, \mathbf{3}_u)$	$(\mathbf{3}_e, \mathbf{3}_u)$
$\mathbf{3}_d$	$(\mathbf{3}_q, \bar{\mathbf{3}}_d)$	$(\mathbf{3}_u, \bar{\mathbf{3}}_d)$	$\mathbf{1} \oplus \mathbf{8}_d$	$(\mathbf{3}_\ell, \bar{\mathbf{3}}_d)$	$(\mathbf{3}_e, \bar{\mathbf{3}}_d)$
$\bar{\mathbf{3}}_d$	$(\mathbf{3}_q, \mathbf{3}_d)$	$(\mathbf{3}_u, \mathbf{3}_d)$	$\bar{\mathbf{3}}_d \oplus \mathbf{6}_d$	$(\mathbf{3}_\ell, \mathbf{3}_d)$	$(\mathbf{3}_e, \mathbf{3}_d)$
$\mathbf{3}_\ell$	$(\mathbf{3}_q, \bar{\mathbf{3}}_\ell)$	$(\mathbf{3}_u, \bar{\mathbf{3}}_\ell)$	$(\mathbf{3}_d, \bar{\mathbf{3}}_\ell)$	$\mathbf{1} \oplus \mathbf{8}_\ell$	$(\mathbf{3}_e, \bar{\mathbf{3}}_\ell)$
$\bar{\mathbf{3}}_\ell$	$(\mathbf{3}_q, \mathbf{3}_\ell)$	$(\mathbf{3}_u, \mathbf{3}_\ell)$	$(\mathbf{3}_d, \mathbf{3}_\ell)$	$\bar{\mathbf{3}}_\ell \oplus \mathbf{6}_\ell$	$(\mathbf{3}_e, \mathbf{3}_\ell)$
$\mathbf{3}_e$	$(\mathbf{3}_q, \bar{\mathbf{3}}_e)$	$(\mathbf{3}_u, \bar{\mathbf{3}}_e)$	$(\mathbf{3}_d, \bar{\mathbf{3}}_e)$	$(\mathbf{3}_\ell, \bar{\mathbf{3}}_e)$	$\mathbf{1} \oplus \mathbf{8}_e$
$\bar{\mathbf{3}}_e$	$(\mathbf{3}_q, \mathbf{3}_e)$	$(\mathbf{3}_u, \mathbf{3}_e)$	$(\mathbf{3}_d, \mathbf{3}_e)$	$(\mathbf{3}_\ell, \mathbf{3}_e)$	$\bar{\mathbf{3}}_e \oplus \mathbf{6}_e$
\vdots	\vdots	\vdots	\vdots	\vdots	\vdots

TABLE I. Example flavour representations of the coupling y in Eq. (1) under $U(3)^5$ (MFV). Uncolored entries denote representations incompatible with an MFV expansion; yellow entries are MFV compatible but correspond to couplings likely too small to reproduce the observed DM relic abundance unless in specific corners of parameter space; green entries are MFV compatible and phenomenologically viable.

couplings to first-generation quarks [3].² On the other hand, constraints involving purely third-generation particles are significantly weaker. This motivates taking a smaller flavour symmetry group as the starting point, which, unlike MFV, permits departures from flavour universality and independent third-generation couplings.

A popular and well-motivated choice is a $U(2)^5$ flavour symmetry, which distinguishes third-generation SM fermions from the first two generations [42, 43, 67–69]. This can be viewed as a subgroup of the full MFV symmetry, under which the SM fermions decompose as

$$\mathbf{3}_f \rightarrow \mathbf{2}_f \oplus \mathbf{1}. \quad (3)$$

This structure is justified by the fact that the third-generation Yukawa couplings are much larger than those of the first two generations, which can be neglected at leading order. In this limit, the full set of SM Yukawas respects an approximate $U(2)^5$ symmetry.

Following the same principles as in MFV, the breaking of $U(2)^5$ induced by the light-quark masses and by CKM mixings can be parametrized in terms of a set of four spurions [43, 70]

$$V_q \sim \mathbf{2}_q, \quad \Delta_u \sim (\mathbf{2}_q, \bar{\mathbf{2}}_u), \quad \Delta_d \sim (\mathbf{2}_q, \bar{\mathbf{2}}_d), \quad \Delta_e \sim (\mathbf{2}_\ell, \bar{\mathbf{2}}_e). \quad (4)$$

The decompositions of MFV spurions from Eq. (2)

² Another typical motivation for $U(2)^5$ over MFV is Drell–Yan production at the LHC, which constrains semileptonic four-fermion interactions with first-generation couplings up to effective scales of $\mathcal{O}(10)$ TeV [64–66].

reads

$$Y_u = \begin{pmatrix} \Delta_u & V_q \\ 0 & y_t \end{pmatrix}, \quad Y_d = \begin{pmatrix} \Delta_d & V_q \\ 0 & y_b \end{pmatrix}, \quad Y_e = \begin{pmatrix} \Delta_e & 0 \\ 0 & y_\tau \end{pmatrix}. \quad (5)$$

The spurions absent from the decomposition, $\mathbf{2}_\ell$, $\mathbf{2}_u$, $\mathbf{2}_d$, and $\mathbf{2}_e$, are phenomenologically constrained to be small.

The representation of the coupling y is then fixed by the $U(2)^5$ transformation properties of f_{SM} and the dark sector field X , and can be expanded in terms of the spurions in Eq. (4). We present several examples in Table II, using the same color coding as in the MFV table.³

A crucial observation is that the representation of y under MFV in Table I can be decomposed under $U(2)^5$ in complete analogy with Eq. (3) and Eq. (5). Since $U(2)^5 \subset U(3)^5$, this implies that some representations that are not compatible with MFV may nevertheless admit a consistent $U(2)^5$ expansion. As a result, such models can become phenomenologically viable.

As an illustrative example, consider the case $X \sim \mathbf{1}$ with $y \sim \mathbf{3}_q$, which we will study in detail in Section 4, and which induces an interaction of the form $y_i \bar{q}_i X$ with $i = 1, 2, 3$. Under $U(2)^5$, this decomposes as $y \sim \mathbf{3}_q \rightarrow \mathbf{2}_q \oplus \mathbf{1}$. The $\mathbf{2}_q$ representation can be constructed from the spurions in Eq. (4), thereby inducing flavour violation, albeit with sufficient suppression. The $\mathcal{O}(1)$ coupling associated with the singlet component involves third-generation fermions and can reproduce the observed relic abundance. Under MFV, no expansion of y in terms of the spurions in Eq. (2) was instead possible, naively ruling out this scenario.

This example also highlights an important point concerning the consistency of the spurion expansion and the necessity of including next-to-leading-order terms. If the gauge representation of X allows couplings to SM fields transforming in different representations of $U(2)^5$, all such couplings must be included, with their sizes fixed by the appropriate powers of the SM spurions when applicable. In the example above, keeping only the coupling to q_3 with $y_3 \sim \mathbf{1} \sim \mathcal{O}(1)$ would be inconsistent. After electroweak symmetry breaking, the rotation to the mass basis induces small couplings to $q_{1,2}$ proportional to CKM matrix elements. At the same order in the $U(2)^5$ expansion, this effect is consistently captured by including couplings of the form $(y_1 \bar{q}_1 + y_2 \bar{q}_2)X$, with $(y_1, y_2) \sim \mathbf{2}_q \sim V_q$.

2.3. Minimal Flavour Protection

One may wonder whether a flavour group even smaller than $U(2)^5$, yet still providing sufficient protection

$X \setminus \bar{f}_{\text{SM}}$	$\bar{\mathbf{3}}_q$		$\bar{\mathbf{3}}_u$		$\bar{\mathbf{3}}_d$...
	$\bar{\mathbf{2}}_q$	$\mathbf{1}$	$\bar{\mathbf{2}}_u$	$\mathbf{1}$	$\bar{\mathbf{2}}_d$	$\mathbf{1}$...
1	$\mathbf{2}_q$	$\mathbf{1}$	$\mathbf{2}_u$	$\mathbf{1}$	$\mathbf{2}_d$	$\mathbf{1}$...
$\mathbf{3}_q$	$\mathbf{1} \oplus \mathbf{3}_q$	$\bar{\mathbf{2}}_q$	$(\mathbf{2}_u, \bar{\mathbf{2}}_q)$	$\bar{\mathbf{2}}_q$	$(\mathbf{2}_d, \bar{\mathbf{2}}_q)$	$\bar{\mathbf{2}}_q$...
	$\mathbf{2}_q$	$\mathbf{1}$	$\mathbf{2}_u$	$\mathbf{1}$	$\mathbf{2}_d$	$\mathbf{1}$...
$\mathbf{3}_u$	$(\mathbf{2}_q, \bar{\mathbf{2}}_u)$	$\bar{\mathbf{2}}_u$	$\mathbf{1} \oplus \mathbf{3}_u$	$\bar{\mathbf{2}}_u$	$(\mathbf{2}_d, \bar{\mathbf{2}}_u)$	$\bar{\mathbf{2}}_u$...
	$\mathbf{2}_q$	$\mathbf{1}$	$\mathbf{2}_u$	$\mathbf{1}$	$\mathbf{2}_d$	$\mathbf{1}$...
$\mathbf{3}_d$	$(\mathbf{2}_q, \bar{\mathbf{2}}_d)$	$\bar{\mathbf{2}}_d$	$(\mathbf{2}_u, \bar{\mathbf{2}}_d)$	$\bar{\mathbf{2}}_d$	$\mathbf{1} \oplus \mathbf{3}_d$	$\bar{\mathbf{2}}_d$...
	$\mathbf{2}_q$	$\mathbf{1}$	$\mathbf{2}_u$	$\mathbf{1}$	$\mathbf{2}_d$	$\mathbf{1}$...
...	⋮	⋮	⋮	⋮	⋮	⋮	⋮

TABLE II. Example flavour representations of the coupling y in Eq. (15) under $U(2)^5$. Subscripts refer to representation under the non-abelian part of $U(2)^5$. The decomposition of the associated MFV representation of \bar{f}_{SM} and X under $U(2)^5$ is also included to highlight the difference in the spurion counting. Color code as in Table I: $U(2)$ -compatible but likely too small for the relic abundance (yellow), $U(2)$ -invariant and viable (green). Leptons are omitted to avoid clutter, but their inclusion is straightforward.

against dangerous flavour violation, can be constructed. The answer is affirmative and goes under the name of Minimal Flavour Protection (MFP), in which the smallest viable flavour symmetry has been identified as [44]

$$SU(2)_q \times U(1)_{x_i}. \quad (6)$$

In this framework, only the first two generations of the left-handed quarks $\mathbf{q} = (q_1, q_2)^T$ transform as a doublet of $SU(2)_q$, while all remaining SM fermions are singlets and carry charges under the additional abelian symmetry $U(1)_{x_i}$.

As shown in [44], $SU(2)_q$ cannot be further reduced, since the large CKM 1-2 mixing induces irreducible flavour violation that unavoidably overshoots either $K - \bar{K}$ or $D - \bar{D}$ mixing bounds, a fact confirmed in our quarkphilic benchmark in Section 4. In addition, a single non-universal flavour group $U(1)_{x_i}$ suffices to control the other sectors. It can be identified with a linear combination of the remaining Cartan generators of $U(3)^5$, *i.e.* $U(1)_{x_i} \subset U(1)^{14}$.⁴

Therefore, under the MFP subgroup, the $U(3)^5$ SM fermion representations decompose as

$$\begin{aligned} \mathbf{3}_{x_q} &\rightarrow \mathbf{2}_{x_q} \oplus \mathbf{1}_{x_{q_3}}, \\ \mathbf{3}_{x_f} &\rightarrow \mathbf{1}_{x_{f_1}} \oplus \mathbf{1}_{x_{f_2}} \oplus \mathbf{1}_{x_{f_3}}, \end{aligned} \quad (7)$$

where $f = u, d, \ell, e$, while the first line is for q . The corresponding $U(1)$ charges are reported as subscripts. The spurions required to reproduce the observed SM masses and mixings consist of three $SU(2)_q$ doublets and a singlet:

$$\mathbf{V} \sim \mathbf{2}_{x_V}, \quad \mathbf{W} \sim \mathbf{2}_{x_W}, \quad \mathbf{U} \sim \mathbf{2}_{x_U}, \quad \mathbf{z} \sim \mathbf{1}_{x_z}. \quad (8)$$

³ While the tensor representations shown technically correspond to the non-Abelian part of the flavour group, the invariance under the $U(1)$ factors is also implicitly assumed [43].

⁴ At the Lie-algebra level, $u(3)_f = \mathfrak{su}(3)_f \oplus \mathfrak{u}(1)_f$. The Cartan subalgebra is three-dimensional and may be chosen as $\{T_3, T_8, X_f\}$, where T_3 and T_8 are the diagonal generators of $\mathfrak{su}(3)_f$ and $X_f \propto \mathbf{1}$ generates $\mathfrak{u}(1)_f$.

The SM charges x_{f_i} and x_{q_3} are expressed in terms of spurion charges (see Table I of [44]) such that Eq. (5) admits the following leading-order form,

$$\begin{aligned}\Delta_u &\sim (\mathbf{V}z^2 \mid \mathbf{W}), \Delta_d \sim (\mathbf{V}z^2 \mid \tilde{\mathbf{V}}z^*), \\ \Delta_e &\sim \begin{pmatrix} z^3 & 0 \\ 0 & z^2 \end{pmatrix}, V_q^{(d)} \sim \mathbf{U}z^*, y_b, y_\tau \sim z,\end{aligned}\quad (9)$$

correctly reproducing the observed SM flavour hierarchies for all spurions of $\mathcal{O}(0.01)$. In addition, the spurion charges can be chosen such that the interaction and mass bases are sufficiently aligned, and that direct spurion insertions yield adequate suppression of SMEFT operators. This was explicitly demonstrated in [44] for the benchmark charge assignment $\{x_V, x_W, x_U, x_z\} = \{1, -2, -3, 7\}$. In general, structural requirements imposed by phenomenological constraints lead to relations among the flavour charges that must always be satisfied. For instance, the charges of q_3 and u_3 must coincide in order to reproduce the large top Yukawa coupling.

As in MFV and $U(2)^5$, the MFP symmetry-spurion framework allows one to systematically construct the allowed flavour structures of the coupling y . In Table III we present several representative examples of the representation of y with the usual colour coding. These illustrate when the flavour symmetry is further reduced from $U(3)^5$ and $U(2)^5$ down to the MFP framework, that new scenarios with sufficient suppression of flavour-violation arise.

A final, important point is that, for appropriate charge assignments of the leptons under $U(1)_{x_i}$, the MFP framework accidentally respects a larger symmetry in the SM charged lepton Yukawa, namely

$$U(1)_e \times U(1)_\mu \times U(1)_\tau, \quad (10)$$

up to a very good approximation. By choosing the charge of X in the t -channel interaction in Eq. (1) such that its coupling to a specific lepton flavour is allowed without spurion insertions (and therefore of $\mathcal{O}(1)$), couplings to the other lepton flavours *necessarily* require insertions of the spurions in Eq. (8). As a result, these couplings are small, strongly suppressing charged-lepton flavour violation, which would otherwise impose severe constraints.

In the presence of multiple t -channel interactions, $\mathcal{L} \supset y^k \bar{f}_{\text{SM}} X^k$, a flavour-protected scenario compatible with DM relic abundance, barring fine-tuned cancellations, requires each coupling y^k to transform as a flavour singlet, $y^k \sim \mathbf{1}_0$, for all k . As an illustrative example, consider a triplet of leptophilic DM χ^k where $k = 1, 2, 3$ and interaction

$$\mathcal{L} \supset y_{ik} \bar{e}_i \chi_k \phi. \quad (11)$$

In the formulation of dark MFV [51], y_{ik} is a new spurion of $U(3)_e \times U(3)_\chi$. Our goal here is to identify the flavour-safe texture of this spurion. Starting from MFV in Table I, and identifying $U(3)_\chi = U(3)_e$, the flavour-singlet coupling $y_{ik} = y \delta_{ik}$ implies universal interactions governed by a single parameter.⁵ Moving to $U(2)^5$, the DM triplet would decompose into

$X \setminus \bar{f}_{\text{SM}}$	$\bar{3}_q$		$\bar{3}_u$...
	$\bar{\mathbf{2}}_q$	$\bar{\mathbf{1}}_{q_3}$	$\bar{\mathbf{1}}_{u_1}$	$\bar{\mathbf{1}}_{u_2}$	$\bar{\mathbf{1}}_{u_3}$	
$3_q \left\{ \begin{array}{l} \mathbf{2}_q \\ \mathbf{1}_{q_3} \end{array} \right.$	$\mathbf{1} \oplus \mathbf{3}_0$	$\bar{\mathbf{2}}_{-q+q_3}$	$\bar{\mathbf{2}}_{-q+u_1}$	$\bar{\mathbf{2}}_{-q+u_2}$	$\bar{\mathbf{2}}_{-q+u_3}$...
	$\mathbf{2}_{q-q_3}$	$\mathbf{1}$	$\mathbf{1}_{u_1-q_3}$	$\mathbf{1}_{u_2-q_3}$	$\mathbf{1}$...
	$\mathbf{2}_{q-u_1}$	$\mathbf{1}_{q_3-u_1}$	$\mathbf{1}$	$\mathbf{1}_{u_2-u_1}$	$\mathbf{1}_{u_3-u_1}$...
$3_u \left\{ \begin{array}{l} \mathbf{1}_{u_1} \\ \mathbf{1}_{u_2} \\ \mathbf{1}_{u_3} \end{array} \right.$	$\mathbf{2}_{q-u_2}$	$\mathbf{1}_{q_3-u_2}$	$\mathbf{1}_{u_1-u_2}$	$\mathbf{1}$	$\mathbf{1}_{u_3-u_2}$...
	$\mathbf{2}_{q-u_3}$	$\mathbf{1}$	$\mathbf{1}_{u_1-u_3}$	$\mathbf{1}_{u_2-u_3}$	$\mathbf{1}$...
	\vdots	\vdots	\vdots	\vdots	\vdots	...

TABLE III. Example flavour representations of the coupling y in Eq. (1) under MFP. The subscripts denote the $U(1)_{x_i}$ charges, while the number in bold identifies the $SU(2)_q$ representation. The decomposition of the associated MFV representation of \bar{f}_{SM} and X under MFP is also included to highlight the difference in the spurion counting. Color code as in Table I: U(2)-compatible but likely too small for the relic abundance (yellow), U(2)-invariant and viable (green). The table can be straightforwardly extended to other cases.

τ -philic singlet and $e\mu$ -philic doublet. Two possibilities with $\mathcal{O}(1)$ couplings arise: a universal coupling in the 1–2 sector with a distinct coupling to the third family, or three independent τ -philic couplings. Other possibilities also exist in which at least one coupling is $\mathcal{O}(1)$, while the others are spurion suppressed. In such cases, the χ^k components with suppressed couplings must be heavier and decay into the component with the $\mathcal{O}(1)$ coupling. Importantly, these decay channels respect the spurion expansion according to the representations of χ^k , consistent with the suppression of flavour violation. This is not restrictive, as even very small couplings suffice to ensure that heavier states decay into the lightest DM state within phenomenologically acceptable timescales.

Finally, within MFP, the DM triplet decomposes into three singlets, each of which may carry one of the x_{e_i} quantum numbers. This results in ten distinct flavour-protected scenarios with $\mathcal{O}(1)$ couplings, allowing all χ^k components to contribute sizably to coannihilations. Again, there are several other viable scenarios in which at least one coupling is $\mathcal{O}(1)$, while the others are controlled by spurions.

Summary — Lowering the assumed flavour symmetry from MFV to $U(2)^5$, and further to the MFP framework, enlarges the space of flavour-protected scenarios for the coupling in Eq. (1). MFV enforces flavour universality up to Yukawa breaking, $U(2)^5$ allows controlled departures associated with the third generation, and MFP admits a broader class of non-universal structures, all while maintaining controlled suppression of flavour violation through symmetry and spurion power counting. The resulting hierarchy of symmetries, $MFP \subset U(2)^5 \subset MFV$, corresponds to an *inverted* hierarchy in the size of the allowed parameter space, as illustrated schematically in Fig. 1.

In what follows, we concentrate on two minimal

⁵ Identifying $U(3)_\chi = U(3)_\ell$ realizes $y_{ik} = (Y_e^\dagger)_{ik}$, which is

flavour-protected but in generic parameter space leads to DM overabundance due to small y_τ .

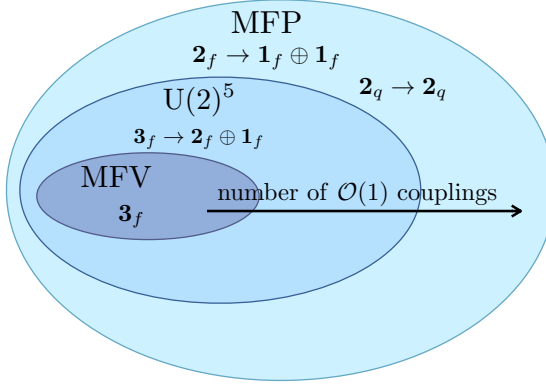


FIG. 1. Schematic illustration of the space of flavour-protected t -channel DM scenarios in different flavour symmetry frameworks.

benchmark configurations discussed in Section 3 and Section 4, which already exhibit rich and distinctive phenomenology and illustrate the general applicability of the framework developed above. The primary goal is to test these expectations for viable flavour structures in the simplest scenarios, leaving a systematic investigation for future studies.

3. Leptophilic Dark Matter

In this section, we focus on a concrete leptophilic scenario in which DM is a complete singlet fermion χ (Dirac or Majorana) and the mediator is a single scalar field Φ carrying the same SM quantum numbers as e_R . The portal interaction is given by

$$\mathcal{L} \supset -y_i \bar{e}_{R,i} \chi \Phi + \text{h.c.} \quad (12)$$

The three components of the coupling vector $\mathbf{y} \sim \mathbf{3}_e$ of $U(3)_e$ break the exact SM lepton flavour symmetry $U(1)_e \times U(1)_\mu \times U(1)_\tau$ and $U(1)_{\chi+\Phi}$ down to a single generalized lepton number $U(1)_L$. These global rotations can be used to remove any complex phase in the vector, implying CP invariance. Hence, we parametrize the components of \mathbf{y} as coordinates on a sphere of radius $y \equiv \|\mathbf{y}\|$, similarly to [58, 59]. This parametrization requires two angles, whose orientation is, in principle, arbitrary. A convenient choice is to use the polar angle θ_τ to quantify the alignment toward a τ -only coupling and the azimuthal angle $\phi_{e\mu}$ to describe the orientation within the $(e\mu)$ plane:

$$\mathbf{y} = y (\sin \theta_\tau \cos \phi_{e\mu}, \sin \theta_\tau \sin \phi_{e\mu}, \cos \theta_\tau). \quad (13)$$

This choice is motivated by the fact that bounds involving τ 's are generally weaker than those involving electrons or muons, as will be shown later, and with this parametrization, the degree of τ alignment becomes immediately apparent. However, this choice is by no means unique. The other two permutations are explored in Appendix B, where we also quantify the degree of μ - and e -alignment, respectively.

The geometry of the parameter space is that of an octant of a sphere, $S^2/(Z_2)^3$, reflecting that the phases in y are unphysical; for this reason, we can

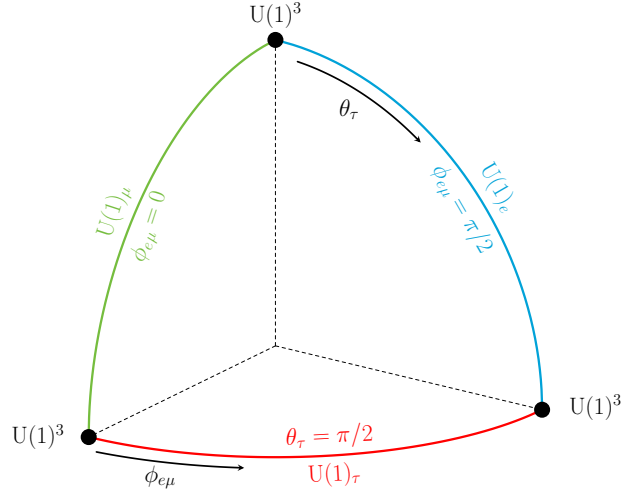


FIG. 2. Visual representation of the parametrization on the octant of the sphere in terms of the polar angle θ_τ and azimuthal angle $\phi_{e\mu}$, and corresponding symmetric limits.

restrict $\theta_\tau \in [0, \pi/2]$ and $\phi_{e\mu} \in [0, \pi/2]$.⁶ It is illustrated in Fig. 2. Along the “meridian” $\phi_{e\mu} = 0$, the coupling to muons vanishes, corresponding to a $U(1)_\mu$ -symmetric limit, while $\phi_{e\mu} = \pi/2$ gives no coupling to electrons, i.e. a $U(1)_e$ -symmetric limit. The “parallel” at $\theta_\tau = \pi/2$ defines the $U(1)_\tau$ -symmetric case. Finally, points naively realizing a $U(1)^2$ limit (such as $\theta_\tau = 0 \leftrightarrow U(1)_e \times U(1)_\mu$) automatically imply full $U(1)^3$ conservation due to the overall $U(1)_L$ preserved by the interaction in Eq. (12), as already discussed in Section 2. This reflects the trivial fact that coupling to a single flavour does not induce any flavour-violating transition.

The various flavour symmetry scenarios introduced in Section 2 can be smoothly explored using this parametrization. Within MFV, the vector $\mathbf{y} \sim \mathbf{3}_e$ does not admit an expansion in terms of SM spurions (see the first row of Table I). Hence, there is no flavour-symmetric parametrization. Within $U(2)^5$, the vector \mathbf{y} can be decomposed as $\mathbf{y} \sim \mathbf{2}_e \oplus \mathbf{1}$. The singlet component, parametrizing the coupling to τ , can consistently be of $\mathcal{O}(1)$. At the same time, in the minimal-breaking scenario, there is no spurion associated with the $\mathbf{2}_e$ representation. This structure realises the $U(1)^3$ limit, represented by the upper corner of Fig. 2.

Finally, within MFP one may couple at $\mathcal{O}(1)$ to any single flavour (electron, muon, or tau) at the time, thereby realising all three corners of Fig. 2. Couplings to the other flavours, corresponding to departures from a given corner, must then be constructed using the spurions in Eq. (8). With the general charge parametrization introduced in [44], the remaining components of the vector y_i are expected to be suppressed by at least two powers of the spurions. For instance, if one chooses to couple to tau with $\mathcal{O}(1)$

⁶ This implies that bounds on $\theta_\tau, \phi_{e\mu}$ are symmetric in shifts of π and with respect to reflections along integer multiples of $\pi/2$.

coupling, the parametrization in Eq. (13) leads to the expectation $\theta_\tau \lesssim 10^{-4}$. Our results show that, if this is the only TeV-scale new-physics sector, the charge assignment of [44] may be relaxed, allowing larger θ_τ .

3.1. Relic Abundance

For Yukawa couplings y_i of order unity, DM candidates in t -channel models can be regarded as WIMP-like particles. As such, they are expected to be in thermal equilibrium in the early universe for $T \gg M_\chi$. Their relic abundance is therefore determined by the thermal freeze-out mechanism [1, 2], where the key quantity is the thermally averaged annihilation cross section of DM pairs into lighter SM states.

Despite its apparent simplicity, thermal freeze-out receives an important modification in t -channel models due to the presence of the mediator Φ , which effectively belongs to the dark sector. When the mediator mass is sufficiently close to the DM mass, more precisely, when the relative mass splitting $\delta_{\text{DM}} \equiv (M_\Phi - M_\chi)/M_\chi$ becomes $\delta_{\text{DM}} \lesssim 0.3$ [2, 71], the mediator remains abundant in the thermal bath during DM freeze-out.⁷ Since the mediator ultimately decays into DM and chemical equilibrium is maintained within the dark sector, coannihilation processes involving fermion–scalar initial states, as well as scalar pair annihilations, must be included to obtain an accurate prediction of the relic abundance.

Coannihilations play an important role in t -channel models [10, 11, 72–77], as well as in generic next-to-minimal WIMP scenarios [2, 78–81]. Complementary bounds from DD and collider searches constrain the $\chi\chi \rightarrow \text{SM SM}$ annihilation rate via crossing symmetry, which may imply that this process is insufficient to deplete the primordial abundance, leading to DM overproduction. Entering the coannihilation regime introduces additional efficient channels for depleting the dark sector population, thereby opening cosmologically viable regions of parameter space.

The effects of the coannihilating particle can still be captured by a single Boltzmann equation [2, 78]

$$\dot{n} = \langle \sigma_{\text{eff}} v_{\text{rel}} \rangle (n^2 - n_{\text{eq}}^2), \quad (14)$$

where n stands for the total number density of the dark sector. The effective cross section is a combination of the various annihilation processes that involve the dark sector states, namely

$$\sigma_{\text{eff}} v_{\text{rel}} = \frac{1}{(\sum_k n_k^{\text{eq}})^2} \sum_{i,j} n_i^{\text{eq}} n_j^{\text{eq}} \sigma_{ij} v_{\text{rel}}, \quad (15)$$

where i, j run over the particles χ and Φ and their complex conjugates. The behavior of the effective cross section in Eq. (15), and its dependence on the

coannihilation channels, can be summarized qualitatively as follows [11] (see [18, 71] for a more detailed expression)

$$\sigma_{\text{eff}} v_{\text{rel}} \sim \sigma_{\chi\chi} v_{\text{rel}} + \sigma_{\chi\Phi} v_{\text{rel}} R + \sigma_{\Phi\Phi} v_{\text{rel}} R^2, \quad (16)$$

where $R = n_\Phi^{\text{eq}}/n_\chi^{\text{eq}} \propto e^{-(M_\Phi - M_\chi)/T}$ is a Boltzmann suppression factor for the processes involving the coannihilating particle Φ , penalizing larger mass splittings.

The cross sections up to order $\mathcal{O}(v_{\text{rel}}^2)$ in the non-relativistic regime relevant for freeze out have been obtained earlier in the literature, see e.g. [11, 17, 82]. Here we briefly summarize the behaviour of the dark fermion pair annihilation cross sections $\sigma_{\chi\chi} v_{\text{rel}}$ and $\sigma_{\chi\bar{\chi}} v_{\text{rel}}$ for the Majorana and Dirac case respectively, which is controlled by the Yukawa coupling. We drop the subscript indicating right-handed chirality of the leptons when writing the relevant processes to avoid clutter. More specifically, the process $\chi\chi \rightarrow e\bar{e}$ receives a helicity suppressed s -wave contribution for Majorana DM, so the velocity suppressed p -wave can in fact dominate at freeze-out.⁸ This is indeed the case for the leptophilic model, where the ratio $(m_\tau/M_\chi)^2 \simeq 2 \times 10^{-3}$ is largest for the smallest DM mass considered in this work ($M_\chi = 45$ GeV) and is quite smaller than $\langle v_{\text{rel}}^2 \rangle \simeq 4 \times 10^{-2}$ at the freeze-out. In contrast, the Dirac case features an s -wave contribution to $\sigma_{\chi\bar{\chi}} v_{\text{rel}}$ that is not helicity suppressed. Therefore, the coannihilation effects are generally more relevant for the Majorana option.

The flavour structure of the Yukawa interaction implies that nine annihilation processes must be considered, namely $\chi\chi \rightarrow e_i\bar{e}_j$ with $i, j = e, \mu, \tau$, and the individual cross sections depend on the mixing angles θ_τ and $\phi_{e\mu}$. However, upon neglecting the lepton masses, which is well justified in the phenomenologically relevant regime $m_\tau/M_\chi \ll 1$, the total annihilation rate becomes flavour independent. Indeed, after summing over all final states, $\sum_{i,j} \sigma v_{\text{rel}}(\chi\chi \rightarrow e_i\bar{e}_j)$, the result no longer depends on the flavour mixing angles. We have checked this for all processes involving the Yukawa interaction, namely also for $\chi\Phi \rightarrow \gamma e_i$, $\chi\Phi \rightarrow Z e_i$, $\Phi\Phi^\dagger \rightarrow e_i\bar{e}_j$ and $\Phi\Phi \rightarrow e_i e_j$. The same applies for the Dirac DM option.

Thermal freeze-out involves non-relativistic particle annihilations. When the annihilating states interact through gauge bosons or scalars, mediating long-range forces, Sommerfeld enhancement [84–86] and bound-state effects [87–89] can significantly modify the annihilation cross sections and affect the relic density prediction. In our work, we include Sommerfeld factors and bound state effects for mediator pair annihilations, namely $\Phi\Phi^\dagger \rightarrow \text{SM SM}'$. For Majorana

⁷ The relative mass splitting needed to significantly affect the DM relic density depends non-trivially on the interplay between the Yukawa coupling y_i and SM gauge couplings.

⁸ We have checked that for right-handed leptons, radiative processes with a photon or a Z boson in the final state, $\chi\chi \rightarrow e\bar{e}\gamma(Z)$, which lift the helicity suppression, remain largely subdominant compared to the $\mathcal{O}(v_{\text{rel}}^2)$ term of the $2 \rightarrow 2$ cross section at freeze out. We have instead included the corresponding radiative process for the quarkphilic scenario, which accounts for corrections of order 10%. Cross sections are taken from [11, 83].

DM, the process $\Phi\Phi \rightarrow ee$ and its conjugate also contribute, which depends solely on the Yukawa coupling. The Sommerfeld factors enhance or suppress the perturbative cross section depending on whether the potential is attractive (for $\Phi\Phi^\dagger$) or repulsive (for $\Phi\Phi$ and $\Phi^\dagger\Phi^\dagger$). The formation of bound states and their decays provides an additional channel for depleting the heavy scalars. Our treatment of near-threshold effects follows the implementations described in [77, 82, 89], consistently accounting for the electroweak crossover that sets the temperature-dependent masses of the electroweak gauge bosons [82, 90]. Since the scalar mediator couples to the SM photon and Z boson with a typical strength $\alpha_{ew} \sim 10^{-2}$, the resulting Sommerfeld and bound-state corrections remain modest, typically at most $\mathcal{O}(10\%)$ level in the relic density prediction. These effects become more pronounced in the quarkphilic scenario, as discussed in Section 4.

It is worth mentioning that we have neglected couplings of the scalar mediator with the Higgs boson in our analysis, focusing instead on the Yukawa interaction in Eq. (1). In general, including such couplings could affect the relic density through additional annihilation channels of the mediator, as well as direct detection and collider searches when the scalar couplings are of order unity (see e.g. [18, 72, 75, 91, 92]), and could also impact the nature of the electroweak phase transition [82, 93].

In our analysis, we compute the DM relic density and restrict the parameter space to reproduce the observed value, $\Omega_{DM}h^2 = 0.1200 \pm 0.0012$ [94]. The resulting parameter space defines targets for the complementary experimental searches discussed below.

3.2. Direct (and Indirect) Detection

Bounds from DD of DM scattering on nuclei arise in the leptophilic context only at the one-loop level. They are directly linked to the requirement that χ constitutes the DM of the universe, and therefore they technically apply only along the relic density contours and for a fixed direction of the coupling vector \mathbf{y} . In t -channel models, the contribution to spin-independent and spin-dependent scattering originates from loop-induced penguin diagrams involving the Higgs boson, the Z , or a photon [95–97]. The dominant one comes from photon penguins, giving rise to the magnetic dipole, charge radius, and anapole operators. At the same time, those involving the Higgs or Z are suppressed by the small lepton masses [17, 95, 98]. Consequently, the resulting bounds from the magnetic dipole moment, which dominate for larger masses, depend primarily on the overall magnitude $y = \|\mathbf{y}\|$ and are nearly independent of the angular parameters.

The Majorana case is special because many of these diagrams sum up to zero as a consequence of the absence of a DM vector current. In this situation, one must rely solely on the anapole moment, which leads to weaker, lepton flavour-dependent bounds [11, 17, 98–100]. Technically, this conclusion is specific to the case of a single DM particle. If multiple flavours of χ were present, the corresponding vector currents

would no longer vanish identically, thereby allowing, in principle, contributions from the other operators. However, for this to occur, the mass splitting between the DM flavours must be smaller than the kinetic energy of non-relativistic DM while still producing a detectable nuclear recoil. This requirement renders the region of parameter space in which this possibility applies somewhat fine-tuned [101].

Concretely, to derive the experimental limits, we employ the expressions for the differential nucleus cross-section given in [17, 98], and follow the procedure outlined in Appendix D of [96] due to the non-trivial dependence on the recoil energy of the various contributions. We use the latest results from the Lux-Zeplin (LZ) experiment [102] at 90% CL, and the projections for DARWIN from [103]. The DD constraints are evaluated along relic density contours by fixing the Yukawa coupling as $y = y(M_\chi, \delta_{DM})$, ensuring self-consistent bounds. The resulting limits are shown in the left panels of Fig. 4 and Fig. 5 for the Majorana and Dirac cases, respectively, and will be discussed in Section 3.5.

Indirect detection probes DM through present day annihilations in astrophysical environments, most notably via γ -ray observations of dwarf spheroidal galaxies, searches for monochromatic γ -ray lines from the Galactic centre, and measurements of the antiproton flux [11, 17, 104, 105]. As reviewed in [10, 11] and confirmed by recent analyses of t -channel models [92, 106], current indirect detection limits are generally weak and do not compete with present or projected DD sensitivities for this class of scenarios.

In leptophilic models, the phenomenology depends strongly on the nature of the DM. For Dirac DM, annihilation into lepton pairs proceeds through an unsuppressed s -wave and indirect searches constrain masses below $\mathcal{O}(100)$ GeV [107], well below the DD reach discussed in Sec. 3.5. For Majorana DM, instead, the s -wave is helicity suppressed by $(m_e/M_\chi)^2$ and the p -wave by v_{rel}^2 with $v_{rel} \approx 10^{-3}$, leading to highly suppressed annihilation rates today [17, 108]. Radiative annihilation $\chi\chi \rightarrow e\bar{e}\gamma$ and loop-induced $\chi\chi \rightarrow \gamma\gamma$ lift this suppression and are constrained by γ -line searches from Fermi-LAT and HESS [107, 109–111]. Using the cross sections from [11, 12], we find no constraints from sharp spectral features in the parameter space consistent with the observed relic abundance.

3.3. Collider Searches

The mediator Φ carries the same quantum numbers as an MSSM right-handed slepton [112]. Therefore, direct searches for supersymmetric sleptons at LEP and the LHC can be directly applied to this scenario [113–119].⁹ These searches are largely independent of the Dirac or Majorana nature of DM.

⁹ For a comprehensive review of t -channel DM searches at LHC, we refer the reader to [10].

At both colliders, sleptons are predominantly pair-produced through electroweak Drell–Yan processes. Most searches target the decay of a slepton into a charged lepton and a neutralino, corresponding precisely to our process $\Phi \rightarrow \ell_i \chi$. These results can thus be straightforwardly reinterpreted, as they depend only mildly on the size of the Yukawa coupling provided that their decay is prompt. Such searches are particularly effective when the mass splitting between Φ and χ is large (tens of GeV) but quickly lose sensitivity in the compressed regime, where the decay products become too soft to be reconstructed efficiently. In that region, the most robust limit arises from measurements of the Z -boson width, which impose $m_\Phi > m_Z/2$. It is plausible that recasting searches designed for compressed chargino–neutralino systems, e.g., [120], could extend the coverage of this region in the slepton-like case, but a dedicated study is beyond the scope of this work.

LEP bounds require some additional care due to the tree-level coupling of Φ to electrons. In this case, Φ can also be produced via t -channel exchange in e^+e^- collisions, which can dominate over the electroweak production if the Yukawa coupling y exceeds the gauge coupling of Φ . Because of the different chiral structures involved, a complete cancellation between the s - and t -channel diagrams cannot occur, so the limits derived here considering only the s -channel can somehow be regarded as conservative.

Finally, the radiative return process $e^+e^- \rightarrow \chi\chi\gamma$, mediated by t -channel Φ exchange, could also provide additional constraints. These bounds depend strongly on the magnitude of the Yukawa coupling y . Adapting the results of Ref. [17] to our setup, we verified that when evaluated along the relic-density contours ($y = y(M_\chi, \delta_{\text{DM}})$) such measurements do not impose any new constraints in the parameter space of the model. Hence, we do not include them in the plots presented in Section 3.5.

3.4. Flavour Observables

Lepton-flavour-violating (LFV) processes provide powerful null tests of the SM. Any observed signal would constitute unambiguous evidence for NP, while negative searches translate into stringent constraints on new mass scales or interactions. Among the many possible probes [121–124], the most constraining are $\mu \rightarrow e\gamma$, $\mu \rightarrow e$ conversion in nuclei, and $\mu \rightarrow 3e$ decays. These observables dominate current limits in the charged-lepton sector and are primary targets of upcoming experiments, notably MEG II [125], Mu2e [126], COMET [127], and Mu3e [128]. Tau decays are currently less constraining for comparable couplings but probe complementary regions of parameter space and are expected to improve with ongoing and future experiments, such as Belle II [129], STCF [130], and FCC-ee [131].

In the t -channel DM scenario considered here, all these processes arise only at the loop level and are further suppressed by a numerically small loop function; explicit expressions are collected in Sections A1

and A2. Despite these suppression factors, LFV observables provide stringent constraints on the parameter space of interest. In Fig. 3, we present the resulting bounds on the mediator mass from $\mu \rightarrow e$ conversion, three-body decays, and radiative transitions, factoring out the dependence on the flavour structure.

The different shades denote bounds corresponding to two choices of the mass splitting between the DM particle and the mediator, shown separately for the Dirac (green) and Majorana (orange) scenarios. Dashed lines indicate future projections. Near mass degeneracy leads to a pronounced suppression in the Majorana case, while the effect is considerably milder for Dirac DM. This behaviour originates from cancellations among box diagrams in the Majorana scenario, whose loop function vanishes in the exact degeneracy limit (see Section A1 and Fig. 10). In contrast, radiative decays and $\mu \rightarrow e$ conversion are governed by the same loop function in both Dirac and Majorana cases and exhibit only a mild suppression as the mass splitting decreases.

Radiative decays $\mu \rightarrow e\gamma$, $\tau \rightarrow e\gamma$, and $\tau \rightarrow \mu\gamma$, with current limits set by MEG II [132], BaBar [133] and Belle [134], provide the most stringent constraints for couplings $y \sim \mathcal{O}(1)$, despite the chirality suppression inherent to these processes. Together with $\mu \rightarrow e$ conversion in nuclei, these observables probe the same parametric combination of couplings $\sim y_i y_j^*/M_\Phi^2$. Future sensitivities for $\mu \rightarrow e\gamma$ and $\mu \rightarrow 3e$ are taken from the MEG II and Mu3e projections discussed above, while the expected reach of COMET II [135] and Mu2e [136] will significantly improve the sensitivity to $\mu \rightarrow e$ conversion. Notably, the latter could surpass the constraints from radiative muon decays in the future.

Three-body decays receive contributions from two distinct parametric structures. In addition to the same $\sim y_i y_j^*/M_\Phi^2$ combination arising from dipole and penguin insertions, they also receive box diagram contributions scaling as $\sim y_i y_j^* y_k y_l^*/M_\Phi^2$ (see Section A2). For $y \lesssim g_{\text{SM}}$ the $\sim y^2/M_\Phi^2$ contribution dominates the three-body amplitude, but it is always more strongly constrained by $\mu \rightarrow e$ conversion and radiative decays than by the three-body channels themselves, both for current bounds and for future projections. As a consequence, three-body decays become phenomenologically relevant only once the box contribution dominates, i.e. when $y \gtrsim g_{\text{SM}}$, for which they effectively probe the quartic coupling structure. Accordingly, in Fig. 3 we show three-body constraints exclusively on the $\sim y^4/M_\Phi^2$ combination, using future sensitivities for τ channels from [41], which include projections from Belle II [129], STCF [130], and FCC-ee [131].

3.5. Interplay and Summary

In this section, we combine the aspects discussed separately in the previous sections, addressing the Majorana and Dirac cases separately due to their distinct features. The main results are presented in Fig. 4 and Fig. 5 for the Majorana and Dirac scenarios, respectively.

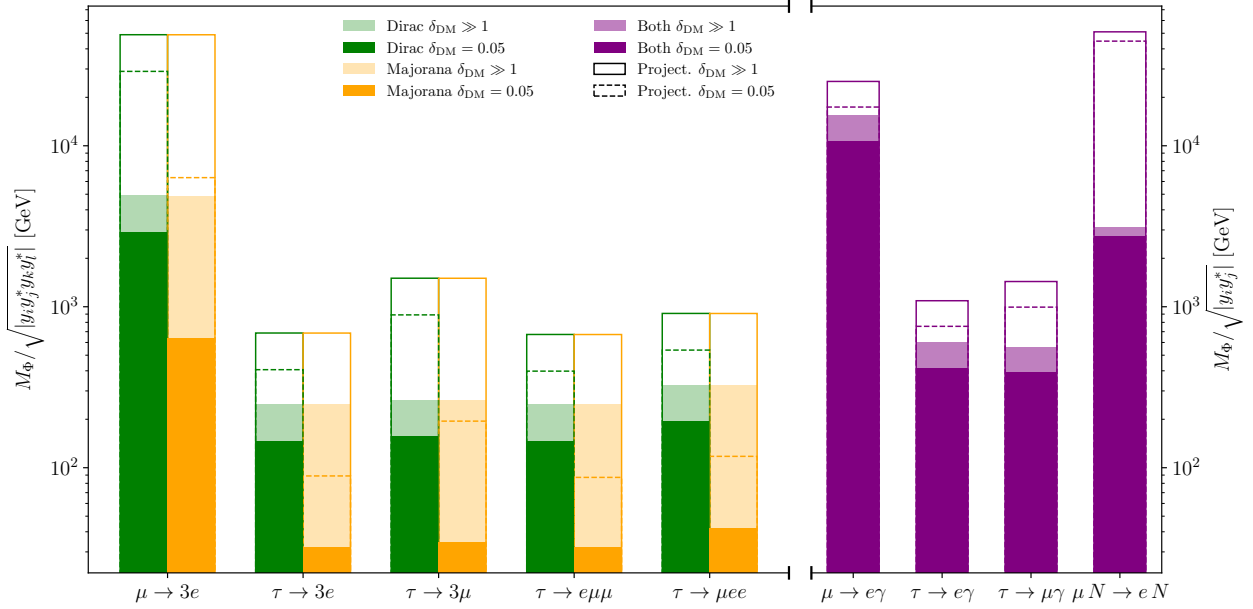


FIG. 3. Leptophilic DM. Bounds on the mediator mass M_Φ from lepton flavour-violating decays, with the dependence on the couplings y_i factored out. On the left-hand side of the plot are the three-body decays, and on the right are the radiative decays. The different shades of the colour correspond to different values of $\delta_{\text{DM}} = (M_\Phi - M_\chi)/M_\chi$, while dashed (solid) lines denote future projections for $\delta_{\text{DM}} = 0.05$ ($\delta_{\text{DM}} \gg 1$). The Dirac and Majorana cases are shown separately on the left. Note that $\delta_{\text{DM}} \gg 1$ corresponds to the limit $M_\chi/M_\Phi \ll 1$ while keeping M_Φ fixed.

The left panels of these figures show constraints from collider searches and DD experiments, together with the parameter space compatible with the observed DM relic abundance. In particular, the grey shaded regions indicate portions of parameter space where reproducing the observed relic abundance requires non-perturbative couplings ($y > \sqrt{4\pi}$) [137], or where the DM relic density falls below the observed value, corresponding to thermal underproduction starting around $y \lesssim g_{\text{SM}}$ (more specifically the hypercharge coupling of the SM). This is due to gauge-driven coannihilations processes $\Phi\Phi^\dagger \rightarrow \text{SM SM}'$, which do not depend on y , and that efficiently depletes the DM whenever the dark fermion and mediator are in chemical equilibrium. In this situation, the correct relic abundance can be obtained only along the line in the $(m_\chi, \delta_{\text{DM}})$ plane denoting the boundary of the underproduction region.¹⁰ Interestingly, near this boundary, the relic abundance becomes essentially independent of the couplings y_i , which can be small. In this regime, complementary constraints from flavour and DD require no particular symmetry alignment and allow for an anarchic flavour structure, unlike when $y \gtrsim g_{\text{SM}}$.

The right panels of Fig. 4 and Fig. 5 show the exploration of the various flavour directions using the basis defined in Eq. (13) in the $(\phi_{e\mu}, \theta_\tau)$ plane for a benchmark point. Using the same colour coding as

a reference, the corresponding flavour-symmetric trajectories and points on the sphere shown in Fig. 2 are also represented. In the plots, a specific benchmark point in $(M_\chi, \delta_{\text{DM}}, y)$ is chosen along the relic abundance contours and highlighted in the left panels by a black star. This benchmark is motivated by its location at the edge of the excluded region and by the non-trivial interplay among the various experimental probes, which we now discuss in detail.

3.5.1. Majorana Dark Matter

In the Majorana case, bounds from DD are very weak, as they arise exclusively from the anapole contribution. Consequently, most of the parameter space evades current direct-detection bounds. However, future DARWIN sensitivity is expected to cut deeply into it, as shown in the left panel of Fig. 4. The model is therefore currently mainly probed by collider searches, which set a lower bound on the DM mass of $\mathcal{O}(100)$ GeV, depending on the splitting, and by flavour constraints. The latter are exhibited in the right panel of Fig. 4 for a benchmark point in parameter space where the DM abundance matches the observed value for $y \simeq 0.98$, with $M_\chi \simeq 170$ GeV and $\delta_{\text{DM}} \simeq 0.14$.¹¹

We observe in the right panel that bounds from flavour transitions vanish as one approaches the

¹⁰ There exists a lower limit below which thermal contact between the mediator and DM is no longer maintained, $y \approx 10^{-7}$. In this regime, coannihilations may still occur without chemical equilibrium between the dark sector states [138, 139], a possibility we do not consider in this work.

¹¹ Although in this benchmark $M_{\chi, \Phi}$ are at the EW scale, the SMEFT calculations presented in the Section A2 are still valid, as discussed there.

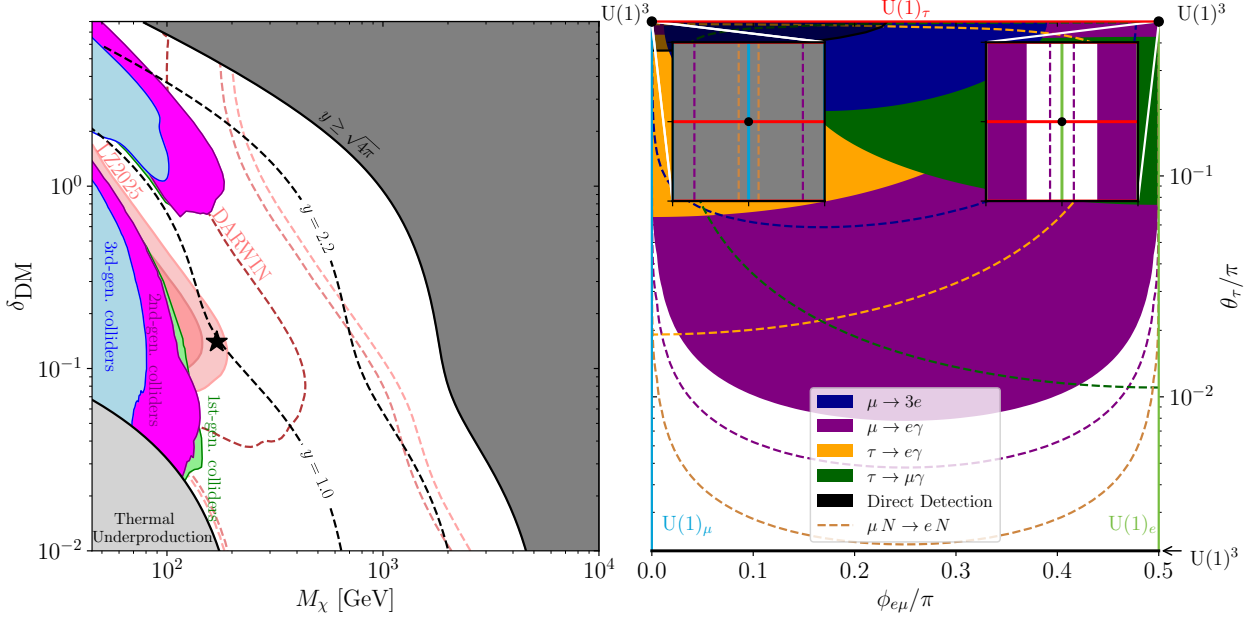


FIG. 4. **Leptophilic Majorana DM.** *Left panel:* Constraints in the $(M_\chi, \delta_{\text{DM}})$ plane, with $\delta_{\text{DM}} \equiv M_\Phi/M_\chi - 1$. Shown are 90% CL bounds from collider searches (green, purple, and blue, corresponding to couplings to first-, second-, and third-generation leptons, respectively), DD (pink, with darker shades indicating couplings to heavier lepton generations; only first- and second-generation bounds are visible), and relic abundance considerations; representative contours for $y = 1$ and $y = 2.2$ are shown. The DD limits are evaluated along relic-density contours with varying couplings. Gray regions indicate parameter space where the coupling required to reproduce the observed relic abundance is non-perturbative, or where the correct abundance cannot be achieved via thermal freeze-out due to overdepletion. Dashed lines denote projected sensitivities from DARWIN. *Right panel:* Constraints from flavour physics and DD in the $(\phi_{e\mu}, \theta_\tau)$ plane, evaluated at the benchmark point indicated by the black star in the left panel ($M_\chi \simeq 170$ GeV, $\delta_{\text{DM}} \simeq 0.14$, $y \simeq 0.98$). Dashed lines denote future projected sensitivities (see Section 3.4). The boxes in the upper-left and upper-right corners show zoomed-in views of the parameter space, illustrating that flavour constraints become ineffective in these regions and that, at the benchmark point, DD excludes the $U(1)_\mu$ limit but not the $U(1)_e$ limit. This region of parameter space is best visualised in Fig. 11. See Section 3.5 for details.

flavour-symmetric limits (see Fig. 2) that forbid the corresponding flavour-violating decay. For instance, $\mu \rightarrow e\gamma$ vanishes at $\phi_{e\mu} = 0, \pi/2$, where $U(1)_\mu$ and $U(1)_e$ are respectively restored, and analogous behaviour is found for the other transitions. Note that this particular choice of angles selects τ flavour over μ and e , as the point at the north pole of the sphere in Fig. 2 is special: for $\theta_\tau = 0$, one gets τ alignment independently of $\phi_{e\mu} \in [0, 2\pi]$. However, this asymmetry is merely an artefact of the chosen parametrisation; the other two bases are plotted in App. B, zooming on the other two corners of Fig. 2. In most of the parameter space, the dominant constraint arises from $\mu \rightarrow e\gamma$, shown in purple. As a result, for a generic azimuthal angle, Fig. 4 shows that τ alignment must be satisfied at the 10^{-2} level. In contrast, Fig. 11 implies significantly stronger bounds for μ - or e -alignment, at the level of 10^{-4} for the benchmark point considered. As a reminder, the maximal misalignment naturally expected in MFP is $\mathcal{O}(10^{-4})$, as discussed at the beginning of Section 3, indicating that current and near-future experiments are beginning to probe the motivated region of parameter space.

We again remark that as the dark sector spectrum becomes increasingly degenerate, the three-body decays are suppressed, as shown in Fig. 10. This suppression weakens the corresponding bounds, making

the radiative decays the only relevant constraints (see Fig. 3). Since radiative decays, both in the Dirac and Majorana DM cases, are only mildly suppressed, and leptonic t -channel DM requires relatively low masses, the process $\mu \rightarrow e\gamma$ always needs some degree of flavour protection. If the model is aligned in either the μ - or e -flavour direction, θ_τ may still remain relatively unconstrained, at least in the more degenerate regimes. This region could be probed by future Belle-II searches for $\tau \rightarrow \ell\gamma$ decays [41, 129, 140], which are expected to explore the parameter space with $\theta_\tau \sim \mathcal{O}(1)$ for both scenarios. Conversely, the model may be aligned in the $\theta_\tau \rightarrow 0$ limit, where the full SM lepton flavour symmetry is restored. In this limit, future experimental sensitivities are expected to improve by roughly an order of magnitude in the branching ratio, translating to a marginally stronger bound of $\theta_\tau/\pi \lesssim 10^{-2}$ for future MEG II projections [141].

Finally, this benchmark highlights the complementarity between flavour physics probes and DD. In particular, DD constrains flavour non-universal but flavour conserving directions compatible with $U(1)_e \times U(1)_\mu \times U(1)_\tau$ symmetric case. The universality is broken by lepton masses as explained in Section 3.2. In contrast, flavour observables are sensitive to the $U(1)^3$ -breaking effects. To show this, in Fig. 4 we

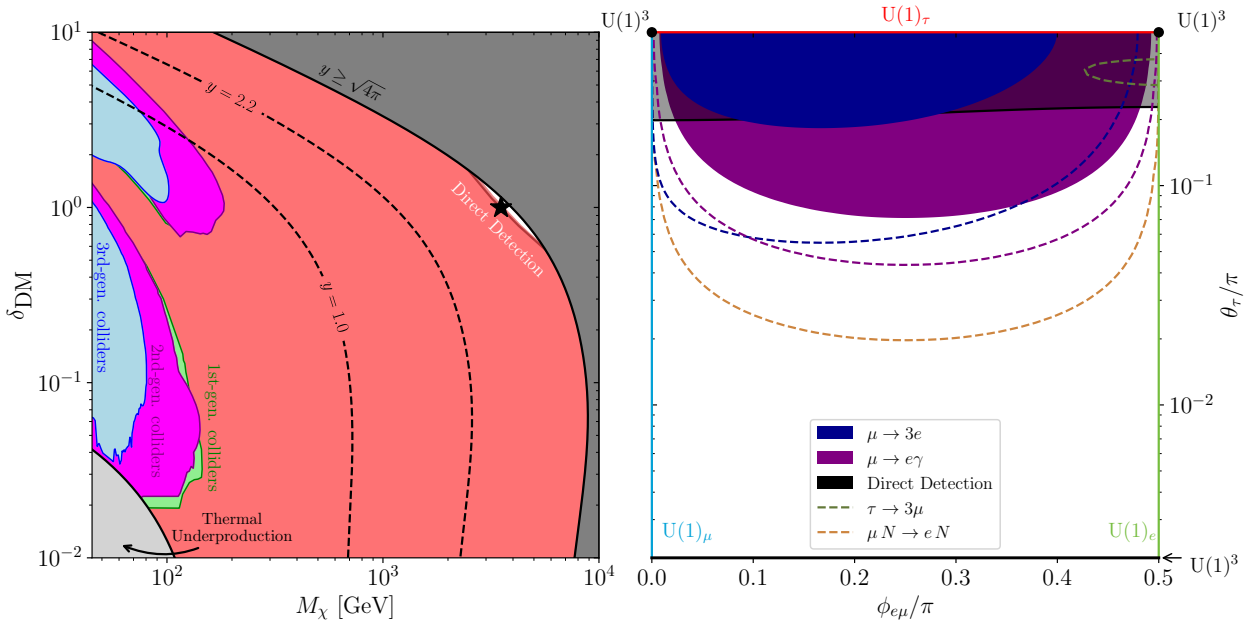


FIG. 5. **Leptophilic Dirac DM.** *Left panel:* Constraints in the $(M_\chi, \delta_{\text{DM}})$ plane, with $\delta_{\text{DM}} \equiv M_\Phi/M_\chi - 1$. Shown are 90% CL bounds from collider searches (green, purple, and blue, corresponding to couplings to first-, second-, and third-generation leptons, respectively), DD (pink, with darker shades indicating couplings to heavier lepton generations; here the bound is essentially the same for all generations), and relic abundance considerations; representative contours for $y = 1$ and $y = 2.2$ are shown. The DD limits are evaluated along relic-density contours with varying couplings. Gray regions indicate parameter space where the coupling required to reproduce the observed relic abundance is non-perturbative, or where the correct abundance cannot be achieved via thermal freeze-out due to overdepletion. *Right panel:* Constraints from flavour physics and DD in the $(\phi_{e\mu}, \theta_\tau)$ plane, evaluated at the benchmark point indicated by the black star in the left panel ($M_\chi \simeq 3.5 \text{ TeV}, \delta_{\text{DM}} \simeq 1, y \simeq 3.35$). Dashed lines denote future projected sensitivities discussed in Section 3.4. See Section 3.5 for details.

have zoomed in on the two respective $U(1)^3$ symmetric points corresponding to coupling to the first or second family only. In this case, DD can completely exclude the e -specific scenario while imposing no constraint on the μ -specific case; see also Fig. 11.

3.5.2. Dirac Dark Matter

The most recent experimental DD limits basically exclude the case of Dirac DM, as shown in the left panel of Fig. 5. The bounds here are stronger because the DM vector current no longer vanishes, leading to the presence of magnetic dipole and charge-radius operators as discussed in Section 3.2. These generate significant spin-independent contributions to DM–nucleus scattering, ruling out the entire parameter space except for a small region around the benchmark point at the edge of perturbativity. This conclusion is flavour-independent. For the benchmark point, DD is shown in gray in the right panel of Fig. 5. Notably, flavour constraints continue to require a degree of alignment with symmetry limits to avoid the $\mu \rightarrow e\gamma$ constraint.

4. Quarkphilic Dark Matter

As a next example, we study a minimal quarkphilic scenario with flavour-singlet χ and Φ coupled to the

left-handed quark doublets:

$$\mathcal{L} \supset -y_i \bar{q}_{L,i} \chi \Phi + \text{h.c.} \quad (17)$$

Since $\mathbf{y} \sim \mathbf{3}_q$ of $U(3)_q$, as before, there is no MFV expansion associated with this coupling (see Table I), which *a priori* hints at $O(1)$ flavour violation. However, it can be decomposed as $\mathbf{3} = \mathbf{2} \oplus \mathbf{1}$ under $SU(2)_q$, in the $U(2)^5$ or MFP framework. Specifically, we can express the expansion according to Table II in terms of the minimal $U(2)_q \subset U(2)^5$ -breaking spurions as

$$\mathbf{y} \sim (aV_q, b) \quad (18)$$

with $\|V_q\| = O(V_{cb})$ defined in Eq. (4), and a, b are $O(1)$ couplings. After the diagonalization of the SM quark mass matrices, this generically results in the structure $\mathbf{y} \sim (\lambda_c^3, \lambda_c^2, 1)$ with λ_c the Cabibbo angle (see also [58, 59]). The same or more suppressed structure could also be realized in the MFP case, depending on the specific $U(1)_{x_i}$ charge assignments.

To test these flavour symmetry hypotheses, we adopt an agnostic angular parametrisation, analogous to that introduced in the leptophilic case:

$$\mathbf{y} = y (\sin \theta \cos \phi e^{i\alpha_1}, \sin \theta \sin \phi e^{i\alpha_2}, \cos \theta). \quad (19)$$

This time we employ the full angular range on the sphere, with $\theta \in [0, \pi]$ and $\phi \in [0, 2\pi]$. The parameters $\alpha_{1,2} \in [-\pi/2, \pi/2]$ represent two irreducible physical CP-violating phases, providing the first qualitative difference with respect to the leptophilic model.

Fixing $y = \|\mathbf{y}\|$, the expansion Eq. (18) implies, generically, that $\cos \phi \sim \lambda_c$ and $\sin \theta \sim \lambda_c^2$, which showcases the typical pattern associated to the U(2) limit.

We choose to define the angular parametrization in Eq. (19) in the down-aligned mass basis, namely in the basis in which the down quark Yukawa matrix is diagonal, which can always be achieved [43]. In this basis, the vector \mathbf{y} in Eq. (19) should be identified with the coupling to down quarks. The corresponding couplings to up quarks are then fixed by the CKM matrix. Explicitly, after diagonalization of the SM Yukawas, one finds

$$\begin{aligned} \mathbf{y}_{\text{down}} &= \mathbf{y}, \\ \mathbf{y}_{\text{up}} &= V_{\text{CKM}} \mathbf{y}. \end{aligned} \quad (20)$$

As a consequence, the interactions with up and down quarks are generically misaligned. This misalignment has important phenomenological implications, as we will see later. It also reflects the fact that, once again, only an $\text{SU}(2)_q$ symmetry on the first two generations provides a meaningful organizing principle for left-handed quark couplings. Indeed, alignment along any of the light generations, corresponding to a U(1) symmetry associated with light left-handed quark flavour numbers, is not well motivated: already in the SM such symmetries are significantly broken by the Cabibbo angle, see Eq. (20). In contrast, in the leptophilic scenario of Section 3, assigning individual lepton flavour numbers is consistent, since treating neutrinos as effectively massless is a good approximation in experiments probing charged-lepton flavour violation.

4.1. Relic Abundance

The discussion of thermal freeze-out for DM interacting with quarks shares many similarities with the leptophilic scenario. As in that case, one must track the abundances of both the DM and the mediator. The main difference is that the scalar Φ now carries full SM gauge charges, introducing several additional annihilation channels for the dark sector states.

A first qualitative difference is that quarks in the final state of the annihilation processes cannot generally be treated as massless. This is particularly relevant for the top quark, whose mass is non-negligible when the DM and mediator masses are of order $\mathcal{O}(1)$ TeV. We anticipate that, for typical DM masses compatible with the observed relic density and still allowed by DD, collider searches, and flavour observables, the ratio m_t/M_χ is in practice relatively small. Nevertheless, it is instructive to highlight that in the quarkphilic case the DM relic abundance becomes *flavour-dependent*, and in particular depends non-trivially on the mixing angle θ .

For illustration, we focus on the Majorana DM pair annihilation process $\chi\chi \rightarrow q_i\bar{q}_j$, with $i, j = 1, 2, 3$ (we again drop the subscript indicating chirality of quarks to avoid clutter.). The corresponding cross sections can be organized into a symmetric 3×3 matrix with six independent entries. Considering only the massive top quark, the 2×2 block associated with the

first and second generations can be computed in the massless limit, where the leading nonvanishing contribution arises from the p wave at order v_{rel}^2 . In contrast, when a third-generation quark, namely its up-type component, enters the final state, the cross section acquires a nonvanishing s -wave contribution. Summing over quark generations yields the following result

$$\begin{aligned} \sum_{i,j=1}^3 \sigma v_{\text{rel}}(\chi\chi \rightarrow q_i\bar{q}_j) &= 2 \sin^4 \theta \sigma_{\chi\chi}^{m_q=0} v_{\text{rel}} \\ &+ 2 \cos^2 \theta \sin^2 \theta (\sigma_{\chi\chi}^{m_q=0} v_{\text{rel}} + \sigma_{\chi\chi}^{m_q} v_{\text{rel}}) \\ &+ \cos^4 \theta (\sigma_{\chi\chi}^{m_q=0} v_{\text{rel}} + \sigma_{\chi\chi}^{2m_q} v_{\text{rel}}). \end{aligned} \quad (21)$$

The first line of eq. (21) corresponds to the first two generations, and the overall factor of two accounts for the $\text{SU}(2)_L$ multiplicity. The second line refers to the non-diagonal entries involving quarks of the first, second, and third generations; here the overall factor of two counts the two possible quark pairs in the final state, $q_i\bar{q}_3$ and $q_3\bar{q}_i$. Finally, the third line accounts for the third generation, where one quark is treated as massless (the bottom quark) and the other as massive (the top quark). Accordingly, $\sigma_{\chi\chi}^{m_q=0} v_{\text{rel}}$, $\sigma_{\chi\chi}^{m_q} v_{\text{rel}}$, and $\sigma_{\chi\chi}^{2m_q} v_{\text{rel}}$ denote the cross sections with zero, one, or two massive quarks in the final state, respectively. Their explicit expressions are given in the Appendix C. In the massless limit, the sum of the cross sections in Eq. (21) reduces to the flavour-blind result found in the leptophilic scenario up to a color factor (see Eqs. (C1) and (C2) for explicit expressions). Accounting for the flavour dependence of the cross sections leads to a modest but noticeable effect on the relic density contours, as illustrated for the Majorana DM scenario in the left panel of Fig. 7 for $\theta = 0$ and $\theta = \pi/2$. A dependence on the quark mass is also induced in the process $\Phi\Phi \rightarrow q_i\bar{q}_j$ in the Majorana dark matter scenario, whose expression is given in Appendix C. For the remaining cross sections, results are available in earlier studies [11, 71, 75, 142].

The second aspect that requires particular care in the quarkphilic scenario is the treatment of near-threshold effects. Due to the interaction of the mediator with QCD gluons, Sommerfeld and bound-state effects are more pronounced than in the leptophilic scenario. Coannihilations of colored particles have been extensively studied in the literature [79, 142–144], and more recently t -channel models have been employed as a test bed to scrutinize bound-state effects and their impact on the relic density of the accompanying DM particle [72–75, 145, 146]. The Sommerfeld factors are largely dominated by QCD-induced interactions, with electroweak contributions typically providing only a subleading correction in the parameter space relevant to the models considered here.¹²

¹² In general, whenever the mediator interacts with QCD gluons, the numerical importance of QCD-assisted coannihilations over the corresponding electroweak contributions can be appreciated by inspecting the mediator–mediator annihilation cross sections.

Scalar pair annihilations can occur in a color singlet, color octet, or color sextet configuration (the latter being relevant only for the Majorana DM option), with an attractive potential in the singlet case and repulsive potentials in the other two cases. The Sommerfeld factors multiply the corresponding color-decomposed annihilation channels; e.g. see [72, 106]. Bound state formation can occur via two main processes, namely radiative emission of a gluon [149–151] and scattering with light plasma constituents [72, 152, 153]. Despite exhibiting a larger rate [72, 152], the latter has been found to give a quite small correction to the DM energy density [153].

To go beyond the minimal inclusion of bound-state effects, namely considering only the ground state, we also include excited states. Their impact can be sizeable [145, 146, 151, 154], particularly depending on the number of excited states included. In this work, we consider four additional states: the $2S$ state and the $2P_m$ states with $m = -1, 0, 1$. While further improvements are possible by including more excited states, this quickly becomes numerically demanding and lies beyond the scope of the present study.¹³ For the quarkphilic case with Majorana DM, neglecting Sommerfeld and bound-state effects leads to order-one differences in the relic density prediction. For instance, for $y = 1.0$ and $\delta_{\text{DM}} = 0.2 (0.05)$, one finds corrections of about 50% (up to a factor of ~ 2.5) in the DM mass range relevant for this work.

4.2. Collider Searches

Similarly to the leptophilic case, collider searches for squarks decaying into SM quarks and neutralinos can be directly applied here. We therefore employ the results from LEP and, most importantly, from the LHC for searches of light-flavour squarks, sbottoms, and stops [116, 156–165]. The light-flavour squarks searches employ untagged jets, so these searches are eventually only sensitive to the angle θ . Since the dominant production mechanism is QCD Drell–Yan pair production, we rescale the experimental limits for several squark flavours to the number of flavours relevant for our setup by adjusting the production cross section, using the cross-sections in Ref. [166]. As in the leptophilic case, there also exists a t -channel diagram for production through couplings to first generation quarks; however, this contribution is subleading for $y \lesssim g_s$, and a complete cancellation with the s -channel process is anyway not possible, so we neglect it. This renders our bounds somewhat conservative.

4.3. Direct (and Indirect) Detection

DD constraints depend on the structure of the coupling vector \mathbf{y} . Couplings to first-generation quarks (u, d) allow for tree-level scattering off nuclei, leading to very strong constraints. For couplings to third-quark generation, the leading one-loop contributions arise from photon, Z , and Higgs penguin diagrams, as in the leptophilic case, together with new box diagrams that generate effective couplings to gluons [95]. Since the Z penguin contributions to DM-nucleus scattering scale as $(m_q/M_\chi)^2$, these effects become particularly relevant for couplings to the top quark.

Regarding the second quark generation, an often overlooked feature in literature is the misalignment implied by Eq. (20). This offset has important consequences for DD, as one cannot realise a pure single-generation alignment. In particular, choosing second family alignment, $(\phi, \theta) = (\pi/2, \pi/2)$, leads to up quark couplings of the form

$$\mathbf{y}_{\text{up}} \sim (\lambda_c, 1, \lambda_c^2), \quad (22)$$

which contains a sizeable first-generation component. This induces a tree-level contribution to DD, leading to very strong constraints on second-family alignment. An analogous discussion, with the roles of up and down quarks interchanged, would apply if one instead chose a basis in which the up quark Yukawa matrix is diagonal.

In the Majorana case, several of the diagrams cancel due to the vanishing DM vector-current $\bar{\chi}\gamma^\mu\chi = 0$ and magnetic dipole $\bar{\chi}\sigma^{\mu\nu}\chi = 0$, resulting in weaker bounds than in the Dirac scenario. In this case, the leading constraints are due to the effective DM-gluon couplings, except for couplings to first-generation quarks, where the spin-dependent cross section sets strong bounds [97]. With third-family coupling, the Higgs exchange is enhanced due to the large top mass; see, for instance, Ref. [75].

To obtain the limits, we take the results of [95, 167] for the analytical expressions of the various contributions, and once again follow the procedure of [96], using the most recent results from LZ [102] and the DARWIN projections [103]. In the Majorana case, the vanishing of vector currents simplifies the procedure, as the dependence on the recoil energy essentially reduces to that employed by the experimental collaborations. As a result, we can directly use the bounds on the spin-independent and spin-dependent nuclear cross sections.

Finally, indirect detection probes DM through present-day annihilations, notably via γ -ray observations of dwarf spheroidal galaxies and the Galactic centre, as well as measurements of the antiproton flux [11, 17, 104, 105]. For t -channel scenarios, current indirect detection bounds are generally weak and remain subdominant to present and projected DD sensitivities [10, 11, 92, 106].

lation cross sections, which scale as g_{SM}^4 [147, 148]. Moreover, Sommerfeld enhancements and bound-state effects become increasingly important for larger values of the coupling constants that induce the long-range interactions [84, 88, 89].

¹³ A very recent work has proposed a numerical tool and public code for incorporating bound-state effects [155], including the possibility of accounting for excited states.

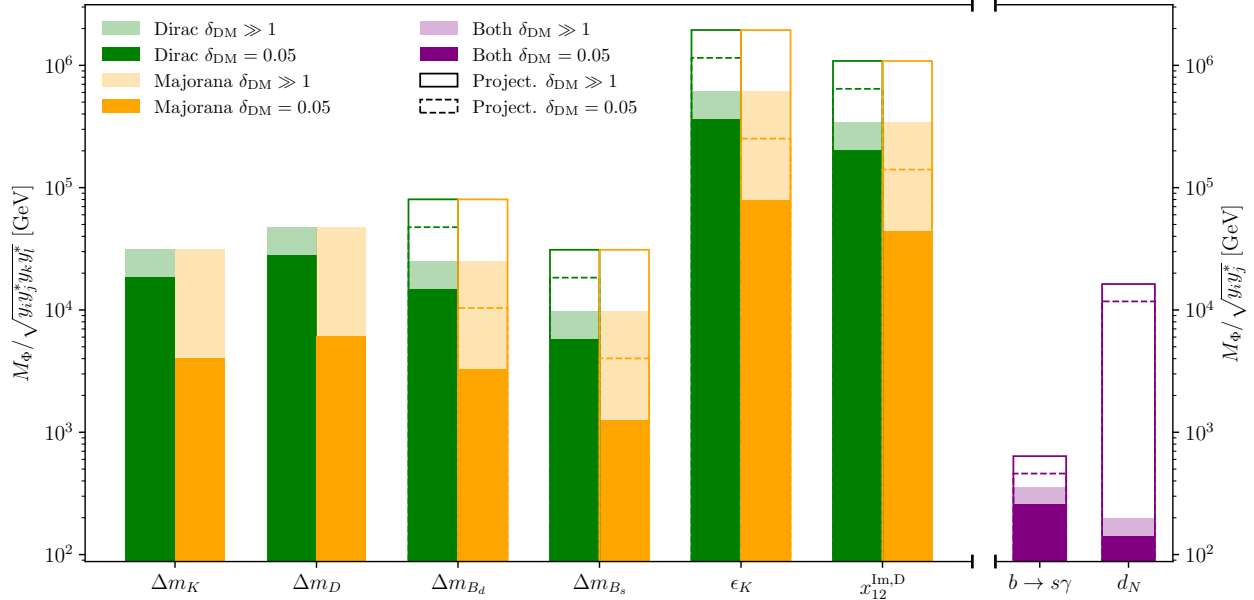


FIG. 6. **Quarkphilic DM.** Bounds on the mediator mass M_Φ from quark-flavour-violating processes, with the dependence on the couplings y_i factored out. On the left hand-side of the plot we report meson-mixing observables, where the bounds refer to the real part of the flavour coefficients for $\Delta m_{K,D}$, to the absolute value for $\Delta m_{B_d,B_s}$ and the imaginary for ϵ_K and $x_{12}^{\text{Im},D}$. Different shades of the colours correspond to different values of $\delta_{\text{DM}} = (M_\Phi - M_\chi)/M_\Phi$. Note that $\delta_{\text{DM}} \gg 1$ corresponds to the limit $M_\chi/M_\Phi \ll 1$ while keeping M_Φ fixed. Shown on the right are the constraint from $b \rightarrow s\gamma$ and d_N . Dashed (solid) lines correspond to future projections for $\delta_{\text{DM}} = 0.05$ ($\delta_{\text{DM}} \gg 1$) following [41].

4.4. Flavour Observables

Quark flavour-changing neutral currents are sensitive probes of NP. Unlike lepton flavour violation, they are suppressed but non-vanishing in the SM, reflecting the approximate nature of quark flavour symmetries. Neutral meson mixings, in particular, are measured with extraordinary precision, making them among the most sensitive tests of NP. Their interpretation, therefore, relies on accurate SM predictions, which are often limited by hadronic uncertainties. In B -meson systems, these arise mainly from lattice determinations of hadronic matrix elements, while in kaon observables such as ϵ_K , additional uncertainties from CKM parameters are relevant.

In our t -channel DM scenario, meson mixing is generated at one loop via box diagrams. Fig. 6 shows the resulting bounds on the mediator mass M_Φ , with the dependence on the couplings y_i factored out, as derived from various flavour observables; details of the extraction are provided in Section A2. Different observables probe different components of the flavour coefficients: ϵ_K and $x_{12}^{\text{Im},D}$ constrain the imaginary parts of the \mathbf{y} vector, $\Delta m_{K,D}$ are sensitive to the real parts, while Δm_{B_q} and ϕ_q depend on both through interference effects. Since the bound from the latter observables are numerically similar, we report in Fig. 6 only the one from Δm_{B_q} . In contrast to the LFV case shown in Fig. 3, bounds from flavour-violating dipole transitions such as $b \rightarrow s\gamma$ are significantly weaker than those induced by four-quark operators. The dependence on the mass splitting is shown for two benchmark scenarios. In the Majorana case, con-

straints from neutral meson mixing become weaker in the small mass-splitting limit, as implied by the behavior of the loop functions shown in Fig. 10. For future projections, we use Fig. 5.15 of Ref. [41] to estimate the improvement factor on the effective scale shown in Fig. 6 for the observables considered, based on the anticipated full datasets in flavor physics, including FCC-ee measurements in the b - and τ -sectors. We add a note of caution that progress in lattice calculations, which is difficult to anticipate, may significantly alter these projections.

Other $\Delta F = 1$ observables beyond dipole transitions are not relevant for our analysis. The reason is that the contributions to the Wilson coefficient C_{10} cancel once all diagrams are consistently included as a consequence of gauge invariance, see Eq. (5.17) of [168]. As a result, potentially stringent probes such as $B_s \rightarrow \mu^+ \mu^-$ do not receive a sizeable contribution. Other flavour observables yield only subleading constraints compared to those already imposed by $b \rightarrow s\gamma$, and are therefore not reported. Note that in our framework, we cannot fit P'_5 because of constraints due to other observables; see Section A2 for more details.

Finally, we comment on bounds from EDMs. These are also sourced from the (chromo-)dipole operators. The rotation to the mass basis induces an electric dipole of up, down, and strange quarks of order $d_q/e \sim m_q \lambda_C \text{Im}[y_1 y_2^*]/16\pi^2 M_\Phi^2$ and similarly for the chromo-electric dipole, see Section A2. With our specific down-aligned choice Eq. (20), only d_u is induced, and leads to the weak constraint $M_\Phi/\sqrt{|\text{Im}y_1 y_2^*|} \gtrsim 200$ GeV at best. Even for $\mathcal{O}(1)$ CP-violating phases,

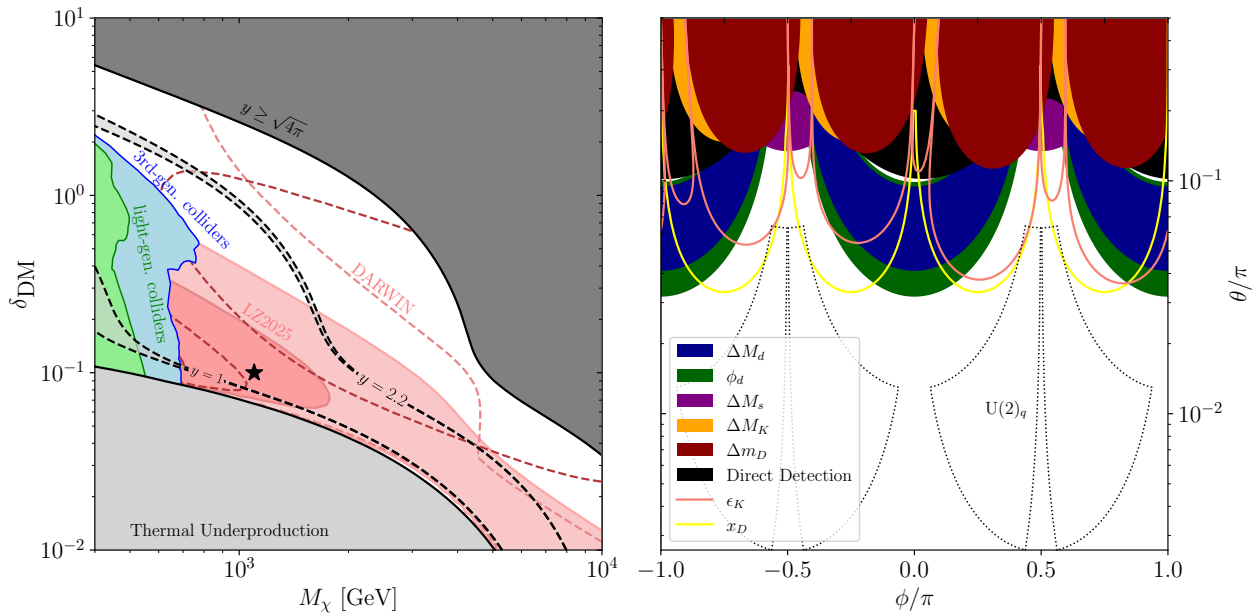


FIG. 7. **Quarkphilic Majorana DM.** *Left panel:* Constraints in the $(M_\chi, \delta_{\text{DM}})$ plane, with $\delta_{\text{DM}} \equiv M_\Phi/M_\chi - 1$. Shown are 90% CL bounds from collider searches (green and blue, corresponding to couplings to light and third-generation quarks, respectively), DD (pink, with darker shades indicating couplings to heavier quark generations), and relic abundance considerations; representative contours for $y = 1$ and $y = 2.2$ are shown. The DD limits are evaluated along relic-density contours with varying couplings. Gray regions indicate parameter space where the coupling required to reproduce the observed relic abundance is non-perturbative, or where the correct abundance cannot be achieved via thermal freeze-out due to overdepletion. Dashed lines denote projected sensitivities from DARWIN. *Right panel:* Constraints from flavour physics and DD in the (ϕ, θ) plane, corresponding to the benchmark point indicated by a black star in the left panel ($M_\chi \simeq 1.1 \text{ TeV}, \delta_{\text{DM}} \simeq 0.1, y \simeq 1.38$). The dotted-black contours encompass regions compatible with a $U(2)_q$ spurion expansion, using $a, b \in [\lambda_c, 5]$ in Eq. (18), as in Ref. [58]. See Section 4.5.1 for details.

the current bound is weaker compared to all the other ones we discussed. However, future projections on EDMs, in particular of the proton, are expected to improve the bound on the overall scale by almost two orders of magnitude [41, 169–171]. Such an improvement could bring the resulting constraint close to that from other flavour observables, as shown in Fig. 6.

4.5. Interplay and Summary

Our main results are presented in Fig. 7 and Fig. 8 for Majorana and Dirac DM, respectively. The plots follow the same conventions as in the leptophilic case: the left panels show constraints from relic abundance, DD, and collider searches in the $(M_\chi, \delta_{\text{DM}})$ plane. The gray region in the left panels corresponding to thermal underproduction is more extended in this case, since in the coannihilation regime the strong interactions of the mediator dilute the DM abundance very efficiently. Bounds from collider searches are also stronger than in the leptophilic case, excluding colored mediator masses $m_\Phi \lesssim 600 \text{ GeV}$. The right panels show flavour bounds in the (ϕ, θ) plane for the specific benchmark point marked by a star in the left panels, that we discuss in detail in the following.

4.5.1. Majorana Dark Matter

DD and flavour observables provide complementary but mutually reinforcing constraints. As shown in the left panel of Fig. 7, DD efficiently excludes large regions of parameter space associated with first- and, to a lesser extent, second-generation couplings, while remaining largely insensitive to a dominantly third-generation alignment. The right panel demonstrates that flavour observables independently point to the same conclusion: generic viable scenarios are driven towards a predominantly third-family structure, allowing only small misalignments. Future improvements in DD sensitivity will play an important role; see DARWIN projections in the left panel.

The right panel of Fig. 7 focuses on a benchmark point $M_\chi = 1.1 \text{ TeV}, \delta_{\text{DM}} = 0.1, y = 1.4$ indicated by a star in the left panel, for which DD already requires a degree of third-family alignment. Flavour observables confirm the need for a coupling structure aligned predominantly with third-generation quarks, with different transitions probing complementary regions of parameter space. Kaon and D -meson mixing constrain angles around $\phi \simeq \pi/4$, where first- and second-generation transitions are maximized, while transitions involving the third generation are most strongly constrained near $\theta \simeq \pi/4$. The strongest limits from B_d mixing arise close to $\phi = 0$, whereas B_s mixing peaks around $\phi = \pi/2$.

A crucial point is that the K - and D -meson con-

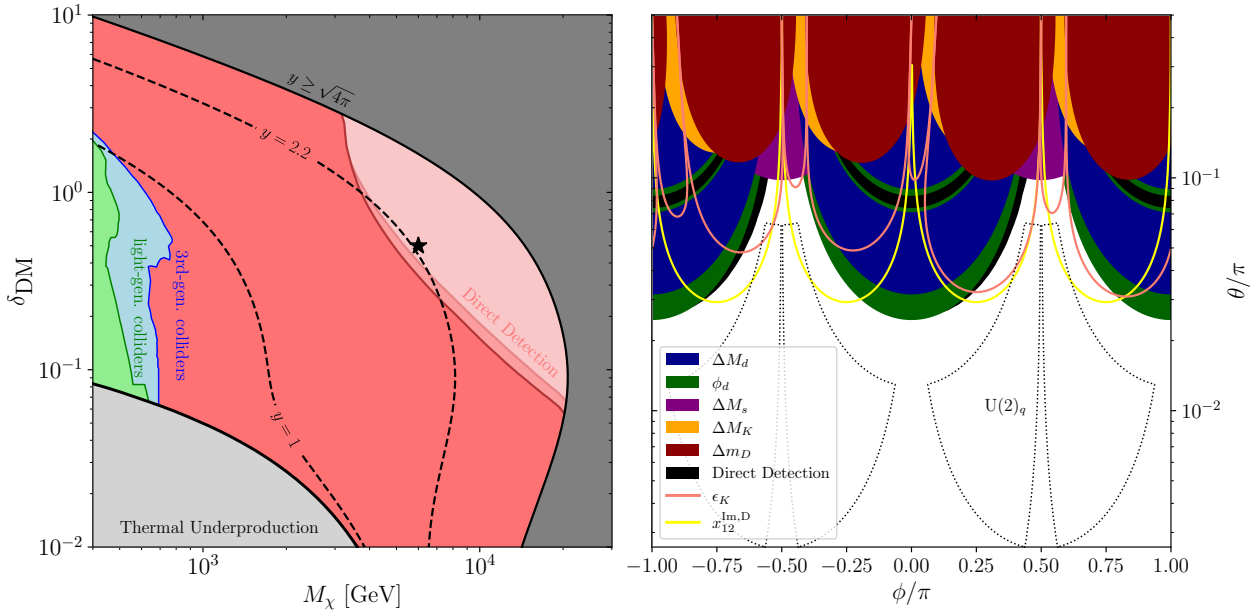


FIG. 8. **Quarkphilic Dirac DM.** *Left panel:* Constraints in the $(M_\chi, \delta_{\text{DM}})$ plane, with $\delta_{\text{DM}} \equiv M_\Phi/M_\chi - 1$. Shown are 90% CL bounds from collider searches (green and blue, corresponding to couplings to light and third-generation quarks, respectively), DD (pink, with darker shades indicating couplings to heavier quark generations), and relic abundance considerations; representative contours for $y = 1$ and $y = 2.2$ are shown. The DD limits are evaluated along relic-density contours with varying couplings. Gray regions indicate parameter space where the coupling required to reproduce the observed relic abundance is non-perturbative, or where the correct abundance cannot be achieved via thermal freeze-out due to overdepletion. *Right panel:* Constraints from flavour physics and DD in the (θ, ϕ) plane, corresponding to the benchmark point indicated by a black star in the left panel ($M_\chi \simeq 6$ TeV, $\delta_{\text{DM}} \simeq 0.5$, $y \simeq 2.26$). The dotted-black contours encompass regions compatible with a $U(2)_q$ spurion expansion. See Section 4.5.2 for details.

straints are not aligned. This follows from the CKM rotation between the up and down quark sectors, Eq. (20). As a consequence, the $U(1)$ limits corresponding to exact alignment with the first or second generation are not viable in the quark sector, since the inevitable rotations proportional to the Cabibbo angle induce excessively large contributions to kaon and D -meson mixing. This resembles what happened also for DD in Section 4.3.¹⁴

In the right panel of Fig. 7, we also highlight the $U(2)_q \subset U(2)^5$ region compatible with the SM spurion expansion Eq. (18), allowing for $\mathcal{O}(1)$ variations, as defined in Ref. [59]. Most of this region remains allowed, demonstrating that a $U(2)^5$ flavour symmetry is compatible with the t -channel DM framework. The same conclusion holds in the MFP framework, with third-family misalignment being equally or more suppressed, depending on the $U(1)_{x_i}$ charge assignment. This behaviour is generic across the parameter space, except in the degenerate limit $\delta_{\text{DM}} \ll 1$, where loop-function suppressions of the relevant SMEFT coefficients permit larger $U(2)_q$ breaking from the minimal spurion scenario. This contrasts with leptophilic t -channel models, where dipole-induced decays domi-

nate and remain unsuppressed in the degenerate limit.

Finally, we assess the impact of CP-violating phases. Choosing $\alpha_2 - \alpha_1 = \pi/4$, which maximises contributions to light-meson observables through $\text{Im}(M_{12}) \propto \sin[2(\alpha_2 - \alpha_1)]$, leads to a substantial strengthening of the bounds. This is consistent with Fig. 6, where CP-violating constraints are roughly an order of magnitude stronger than CP-conserving ones. Nevertheless, the plot demonstrates that the $U(2)_q$ flavour-spurion structure is sufficient, without the need to impose an additional CP symmetry.

Overall, the case of Majorana DM with a left-handed quarkphilic mediator represents an interesting scenario, exhibiting a non-trivial interplay between DD and flavour bounds. Our results confirm the expectation that a certain degree of alignment with the third generation is required in most of the parameter space, which can be naturally embedded in a $U(2)^5$ or MFP flavour framework.

4.5.2. Dirac Dark Matter

The quarkphilic Dirac case is significantly more constrained. As shown in Fig. 8, DD bounds are extremely strong in this scenario, to the extent that models with couplings to first-generation quarks are essentially excluded. Alignment towards the heavier generations is also strongly constrained, due to the enhanced Z -penguin and dipole contributions to DM-nucleus scattering in the Dirac case. As a result, only

¹⁴ Instead, for DM coupled to right-handed u_R or d_R , the MFP framework of Section 2.3 suggests that the corresponding $U(1)$ limits could be viable, similarly to the leptophilic case, since it would correspond to removing either up- or down-type of meson-mixing observables in Figs. 7 and 8.

a small region of parameter space remains viable, corresponding to large couplings close to the perturbativity bound ($y \gtrsim 2$). Such large couplings are prone to the development of Landau poles at relatively low scales [92], suggesting the need for a low-scale completion of the model.

The flavour bounds are shown in the right panel of Fig. 8 for a benchmark point $M_\chi = 1.1$ TeV, $\delta_{\text{DM}} = 0.1$, and $y = 1.38$. The considerations are similar to those in the Majorana case: flavour observables require a degree of alignment towards the third generation, as naturally realized in $U(2)^5$ or MFP frameworks. A difference at small mass splittings, originating from the fact that for Dirac DM the loop functions entering meson mixing remain non-vanishing even in the degenerate limit, is phenomenologically irrelevant here, since this region of parameter space is already excluded by DD constraints.

In summary, the case of Dirac DM with a left-handed quarkphilic mediator is almost excluded by DD, except for scenarios with couplings close to the non-perturbative regime.

5. Conclusion

In this work, we have examined thermal DM in t -channel models through the lens of flavour physics. These scenarios constitute a well-motivated and minimal extension of the WIMP paradigm, featuring renormalisable interactions between DM, a mediator, and SM fermions. Reproducing the observed relic abundance naturally points to TeV-scale masses and $\mathcal{O}(1)$ couplings. As a result, such models generically induce flavour- and CP-violating effects, bringing them under the stringent scrutiny of precision flavour observables. Ensuring consistency with existing flavour bounds, therefore, emerges as a central consistency requirement for t -channel DM.

We addressed this question systematically by adopting the framework of flavour symmetries and spurion expansions presented in Section 2. By classifying the DM and mediator fields and their couplings under different flavour symmetry hypotheses, we provided a structured map of viable flavour scenarios for t -channel models. This generalises the logic of MFV, provides a clear dictionary for identifying which flavour structures can realistically be consistent with existing bounds, and establishes a basis for future comprehensive studies of flavour in dark sectors. In practice, the flavour-singlet entries in Table I, Table II, and Table III serve as bottom-up simplified-model benchmarks for further investigation. As summarised in Fig. 1, progressively reducing the flavour symmetry,

$$\text{MFV} \rightarrow U(2)^5 \rightarrow \text{MFP}, \quad (23)$$

opens up a substantially broader class of viable t -channel DM scenarios.

To quantitatively test these symmetry expectations, we focused on simple yet representative benchmark scenarios in which both the DM particle and the mediator are flavour singlets. This choice leads

to *rank-1 flavour violation* in the couplings, parameterised by angular variables in Eq. (13) and Eq. (19), and admitting a convenient geometric representation on the sphere shown in Fig. 2. Symmetry limits then correspond to specific points or trajectories on this sphere. Rather than imposing these limits a priori, we performed an agnostic phenomenological analysis, using the full set of available experimental constraints to determine how closely viable models must align with flavour symmetry directions. We studied two concrete realisations: interactions with right-handed charged leptons in Section 3 and with left-handed quarks in Section 4, considering both Dirac and Majorana DM.

In the leptophilic scenario, Majorana DM remains largely viable and mostly unexplored, as illustrated by the left panel of Fig. 4, where sizable regions of parameter space survive all current constraints. As anticipated, the allowed flavour directions are organised by approximate lepton flavour number symmetries: viable scenarios require alignment with a single lepton flavour, with couplings to the third generation being somewhat less constrained, as shown in the right panel of Fig. 4. By contrast, the Dirac leptophilic case, summarised in Fig. 5, is essentially excluded by DD for all flavour directions. This conclusion relies critically on the latest results from LUX-ZEPLIN [102].

In the quarkphilic scenario, we observe a rich interplay between flavour observables and DD. For Majorana DM, summarised in Fig. 7, a sizeable region of parameter space remains viable. As anticipated, flavour constraints demand alignment with the third quark generation, pointing to an underlying $SU(2)_q$ flavour symmetry. Frameworks such as $U(2)^5$ or MFP naturally realise this alignment, efficiently suppressing flavour violation through small spurions while still reproducing the observed relic abundance, as illustrated in the right panel of Fig. 7. By contrast, the Dirac quarkphilic scenario is far more constrained as shown in Fig. 8: DD limits are particularly stringent and require both a highly restrictive flavour structure, again well captured by an $SU(2)_q$ symmetry, and a large third-generation coupling close to the perturbativity limit.

For both scenarios considered, and in particular for the quarkphilic case, the inclusion of Sommerfeld enhancements and bound-state effects is essential to obtain an accurate determination of the relic density when the mass splitting between the DM and the mediator is moderate or small.

Overall, our results highlight a clear picture: t -channel DM models generically require a non-trivial flavour structure to evade flavour bounds, and flavour symmetries presented in Section 2 provide a well-motivated guiding principle to identify viable scenarios. At the same time, DD experiments play a crucial complementary role by probing the flavour-conserving components of the same couplings. In this sense, flavour physics points to the allowed directions in flavour space, while DD constrains their overall size.

With the progress in DD experiments, the landscape of t -channel fermionic DM models is coming into sharper focus: Dirac DM has already been excluded or pushed to the brink of viability, thereby

shifting attention to Majorana DM in the next generation of experiments. Precision flavour measurements at present and future colliders [41] will continue to probe ever smaller departures from flavour symmetry limits. At the same time, collider searches at the HL-LHC and electroweak precision measurements at FCC-ee [92] will provide complementary probes. Together, this multi-front experimental programme will test the viability of thermal DM at the TeV scale.

Acknowledgments

We thank Daniel Naredo-Tuero, Pablo Olgoso, and Stefan Vogl for helpful discussions. This work was supported by the program “Swiss High Energy Physics for the FCC” (CHEF).

A. SMEFT Matching and Flavour Observables

In this section, we report the relevant one-loop matching expressions of the benchmark models to the effective operators inducing quark and lepton flavour observables, as well as the formulae of the observables considered in this analysis.

A1. Matching to the SMEFT

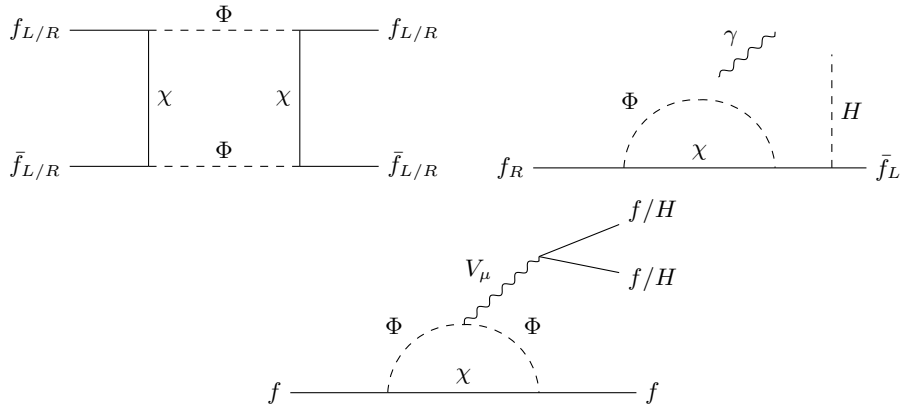


FIG. 9. Representative Feynman diagrams generating the four-fermion and \mathcal{O}_{He} operators (box and penguins, left and bottom) and the dipole operators (right) for quarks and leptons. Diagrams were drawn using **FeynCraft** [172].

After integrating out at one-loop the heavy mediator and DM candidate, we end with the following relevant subset of SMEFT operators for the leptophilic scenario

$$\begin{aligned} \mathcal{L}_{\text{EFT}}^e &= \mathcal{C}_{eB}\mathcal{O}_{eB} + \mathcal{C}_{He}\mathcal{O}_{He} + \mathcal{C}_{ee}\mathcal{O}_{ee} + \mathcal{C}_{\ell e}\mathcal{O}_{\ell e} + \mathcal{C}_{qe}\mathcal{O}_{qe} + \mathcal{C}_{eu}\mathcal{O}_{eu} + \mathcal{C}_{ed}\mathcal{O}_{ed} \\ &= [\mathcal{C}_{eB}]_{ij} \bar{\ell}_i H \sigma_{\mu\nu} e_j B^{\mu\nu} + [\mathcal{C}_{He}]_{ij} \bar{e}_i \gamma^\mu e_j (H^\dagger i \overleftrightarrow{D}_\mu H) \\ &\quad + [\mathcal{C}_{ee}]_{ijkl} \bar{e}_i \gamma^\mu e_j \bar{e}_k \gamma_\mu e_l + [\mathcal{C}_{\ell e}]_{ijkl} \bar{\ell}_i \gamma^\mu \ell_j \bar{e}_k \gamma_\mu e_l \\ &\quad + [\mathcal{C}_{qe}]_{ijkl} \bar{q}_i \gamma^\mu q_j \bar{e}_k \gamma_\mu e_l + [\mathcal{C}_{eu}]_{ijkl} \bar{e}_i \gamma^\mu e_j \bar{u}_k \gamma_\mu u_l + [\mathcal{C}_{ed}]_{ijkl} \bar{e}_i \gamma^\mu e_j \bar{d}_k \gamma_\mu d_l, \end{aligned} \quad (\text{A1})$$

while for the quarkphilic scenario

$$\begin{aligned} \mathcal{L}_{\text{EFT}}^q &= \mathcal{C}_{d(u)B}\mathcal{O}_{d(u)B} + \mathcal{C}_{d(u)W}\mathcal{O}_{d(u)W} + \mathcal{C}_{d(u)G}\mathcal{O}_{d(u)G} + \mathcal{C}_{qq}\mathcal{O}_{qq}^{(1)} \\ &= [\mathcal{C}_{d(u)B}]_{ij} \bar{q}_i H \sigma_{\mu\nu} d_j B^{\mu\nu} + [\mathcal{C}_{d(u)W}]_{ij} \bar{q}_i H \sigma_{\mu\nu} \tau^a d_j W^{a\mu\nu} \\ &\quad + [\mathcal{C}_{d(u)G}]_{ij} \bar{q}_i H \sigma_{\mu\nu} T^A d_j G^{A\mu\nu} + [\mathcal{C}_{qq}]_{ijkl} \bar{q}_i \gamma^\mu q_j \bar{q}_k \gamma_\mu q_l. \end{aligned} \quad (\text{A2})$$

Note that we do not include any $\Delta F = 1$ operators beside dipoles; see the end of Section A2 for the explanation. In Fig. 9, we show the corresponding diagrams that generate the four-fermion, penguin, and dipole operators. Starting from Eqs. (12) and (17), we perform the matching onto the corresponding Wilson coefficients using **Matchete** [173]. For the leptophilic scenario, the result can be written as

$$[\mathcal{C}_{eB}]_{ij} = \frac{g'}{384\pi^2 M_\Phi^2} y_i y_k^* Y_{kj} G(x_\Phi), \quad [\mathcal{C}_{He}]_{ij} = -\frac{g'^2}{576\pi^2 M_\Phi^2} y_i y_j^* H(x_\Phi), \quad (\text{A3})$$

$$[\mathcal{C}_{ee}]_{ijkl} = \frac{1}{64\pi^2 M_\Phi^2} \left[-\frac{1}{2} y_i y_j^* y_k y_l^* F(x_\Phi) + \frac{g'^2}{9} (\delta_{ij} y_k y_l^* + \delta_{il} y_j^* y_k) H(x_\Phi) \right], \quad (\text{A4})$$

$$[C_{\ell e}]_{ijkl} = \frac{g'^2}{576\pi^2 M_\Phi^2} \delta_{ij} y_k y_l^* H(x_\Phi), \quad [C_{qe}]_{ijkl} = -\frac{g'^2}{1728\pi^2 M_\Phi^2} \delta_{ij} y_k y_l^* H(x_\Phi), \quad (\text{A5})$$

$$[C_{eu}]_{ijkl} = -\frac{g'^2}{432\pi^2 M_\Phi^2} \delta_{kl} y_i y_j^* H(x_\Phi), \quad [C_{ed}]_{ijkl} = \frac{g'^2}{864\pi^2 M_\Phi^2} \delta_{kl} y_i y_j^* H(x_\Phi), \quad (\text{A6})$$

while for the quarkphilic scenario

$$[C_{qq}^{(1)}]_{ijkl} = -\frac{1}{128\pi^2 M_\Phi^2} y_i y_j^* y_k y_l^* F(x_\Phi), \quad [C_{u(d)B}]_{ij} = -\frac{g'}{2304\pi^2 M_\Phi^2} y_i y_k^* Y_{u(d),kj} G(x_\Phi), \quad (\text{A7})$$

$$[C_{u(d)W}]_{ij} = -\frac{g}{768\pi^2 M_\Phi^2} y_i y_k^* Y_{u(d),kj} G(x_\Phi), \quad [C_{u(d)G}]_{ij} = -\frac{g_s}{384\pi^2 M_\Phi^2} y_i y_k^* Y_{u(d),kj} G(x_\Phi), \quad (\text{A8})$$

with $x_\Phi = M_\chi^2/m_\Phi^2$, and the loop functions given by

$$G(x_\Phi) = \frac{1}{(1-x_\Phi)^4} [(1-x_\Phi)(1-x_\Phi(5+2x_\Phi)) - 6x_\Phi^2 \log x_\Phi] \quad (\text{for dipoles}), \quad (\text{A9})$$

$$H(x_\Phi) = \frac{1}{2(1-x_\Phi)^4} [(1-x_\Phi)(2-x_\Phi(7-11x_\Phi)) + 6x_\Phi^3 \log x_\Phi] \quad (\text{for penguin}), \quad (\text{A10})$$

$$F_D(x_\Phi) = \frac{1}{(1-x_\Phi)^3} [1 - x_\Phi^2 + 2x_\Phi \log x_\Phi] \quad (\text{for box, } \chi \text{ Dirac}), \quad (\text{A11})$$

$$F_M(x_\Phi) = \frac{1}{(1-x_\Phi)^3} [1 + 4x_\Phi - 5x_\Phi^2 + 2x_\Phi(2+x_\Phi) \log x_\Phi] \quad (\text{for box, } \chi \text{ Majorana}), \quad (\text{A12})$$

The loop functions satisfy

$$\{G(x_\Phi), H(x_\Phi), F_D(x_\Phi), F_M(x_\Phi)\} \xrightarrow{x_\Phi \rightarrow 0} 1, \quad (\text{A13})$$

$$\{G(x_\Phi), H(x_\Phi), F_D(x_\Phi), F_M(x_\Phi)\} \xrightarrow{x_\Phi \rightarrow 1} \left\{ \frac{1}{2}, \frac{3}{4}, \frac{1}{3}, 0 \right\}. \quad (\text{A14})$$

The behaviour of the loop functions can also be seen in Fig. 10, which shows that the Majorana loop function F_M vanishes in the degenerate limit.

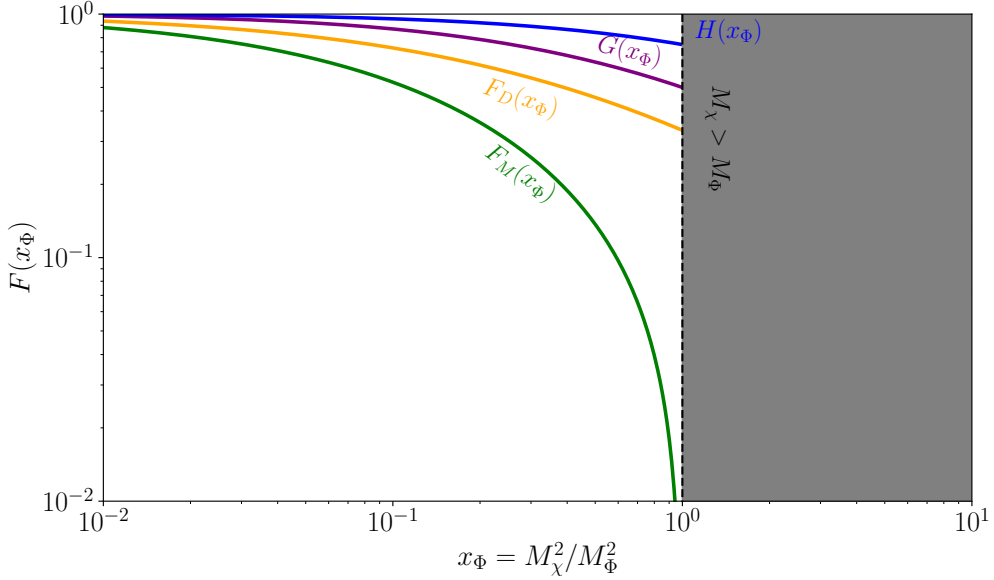


FIG. 10. Loop functions for the 4-fermion operators and dipoles, in terms of the mass ratio $x_\Phi \equiv M_\chi^2/M_\Phi^2 = (1+\delta_{\text{DM}})^{-2}$.

A2. Flavour Observables

Leptons. — The class of observables considered in Section 3 includes flavour-violating three-body lepton decays, $\mu \rightarrow e$ conversion in nuclei, and dipole transitions $\ell_i \rightarrow \ell_j \gamma$. The expressions for these observables in terms of the Wilson coefficients listed in Section A1 are well known in the literature and will not be reported here, see for example [123, 174]. We limit ourselves to a few remarks:

- in the spin-independent contribution to $\mu \rightarrow e$ conversion, the dipole, four-fermion, and C_{He} operators induce an effective vector coupling only to protons. This follows from the fact that these contributions are dominated by photon exchange or by scalar operators matched onto the electromagnetic current, which does not couple coherently to neutrons. This observable constrains the combination $\sim y^2/M_\Phi^2$;
- dipole transitions $\ell_i \rightarrow \ell_j \gamma$ are likewise sensitive to the same parametric combination $\sim y^2/M_\Phi^2$;
- three-body decays receive contributions scaling both as $\sim y^4/M_\Phi^2$, from four-lepton box diagrams, and as $\sim y^2/M_\Phi^2$, from dipole and penguin ones. Given the current experimental bounds from $\mu \rightarrow e$ conversion and dipole transitions, the bound from three-body decay constraints on the latter combination is subleading. The same also holds when comparing future projections.

Note that we compute the observables by matching the SMEFT onto the LEFT, integrating out the heavy Z , W , and Higgs bosons, and expressing the observables in terms of the resulting LEFT Wilson coefficients. We stress that, in the scenario considered here, this procedure remains valid even when $M_{\Phi,\chi}$ are around or below the electroweak scale. In fact, one could equivalently match directly onto the LEFT and obtain the same result. This follows from two observations. First, the relevant momentum transfer in the processes of interest is $q^2 \lesssim m_\tau^2 \ll m_Z^2$. Second, the dark sector does not couple directly to the Higgs, so no corrections to Eq. (A1) featuring powers of $|H|^{2n}$ are present, which after electroweak symmetry breaking could invalidate the EFT expansion.

An alternative way to see this is to note that the operators in Eq. (A1) proportional to $g'^2 y^2$ are actually obtained from operators such as $(\bar{e}\gamma_\mu e)\partial_\nu B^{\mu\nu}$ after applying the equation of motion $\partial_\nu B^{\mu\nu} = J_Y^\mu$, reducing them to Higgs-fermion current and four-fermion interactions. The same operators with a photon or Z fields could be matched directly after electroweak symmetry breaking, and would not get corrected by powers of $m_Z^2/m_{\Phi,\chi}^2$.

Quarks. — Unlike in the LFV case, where the SM prediction for flavour violation is effectively zero, in the quark sector, the SM uncertainties must be determined precisely. However, in most cases, the SM predictions are dominated by hadronic and CKM-related uncertainties, which propagate into the observables and typically exceed the experimental errors. In the remainder of this section, we summarise the inputs used to compute both the SM and NP contributions to the various flavour observables.

Firstly, since our NP contributions enter through meson mixing, these processes cannot be used to determine the CKM matrix. Instead, we adopt the PDG [175] determination of the CKM elements obtained exclusively from tree-level observables, which our model does not modify. This tree-level determination comes with larger uncertainties, as B -meson mixing is otherwise very precisely measured. We have assessed the impact of using different CKM inputs, particularly the dependence on the V_{cb} determination from inclusive versus exclusive decays. We find that adopting the inclusive value leads to better agreement with the SM predictions, especially for ϵ_K , consistent with Ref. [176], and fully compatible with the use of the tree-level CKM. In our analysis, we have also investigated the effect of performing a simultaneous fit of the CKM parameters, including both meson mixing observables and potential NP contributions. This approach yields results similar to those obtained using the tree-level CKM, and we therefore employ meson mixing primarily to extract bounds on NP. Consequently, we find that using the PDG tree-level CKM determination provides a straightforward and robust implementation, consistent within the corresponding confidence intervals.

For meson mixing, we use the recent Kaon bag parameter from Ref. [177], and for the B -mesons we adopt the bag parameters and decay constants from Ref. [178]. The detailed procedure and explicit expressions for the QCD running and the computation of the hadronic matrix elements can be found in Appendix C of Ref. [179], which follows the analyses of the UTfit collaboration [180–182]. In our numerical evaluation, we make use of the Wilson-coefficient bag parameters from Refs. [178, 183, 184].

Finally, to compute the relevant observables, we adopt the following approximations. For K -meson mixing, the contribution to the mass splitting is given by the real part of the amplitude,

$$\Delta m_K \simeq 2\text{Re} (M_{12}^{\text{SM}} + M_{12}^{\text{NP}}), \quad (\text{A15})$$

where M_{12} denotes the (short-distance) dispersive part of the mixing Hamiltonian. Currently, no reliable estimate of the long-distance effects is available. Therefore, we simply require the NP contribution not to exceed the SM short-distance contribution [185], ensuring compatibility with experimental values. In the case of D -mesons, long-distance effects are expected to dominate; thus, our conservative approach is to demand that the NP contribution does not overshoot the experimental measurements [175].

However, for CP-violating observables such as ϵ_K and $x_{12}^{\text{Im},D}$, the SM predictions are better understood. In particular, there exists a precise SM prediction for ϵ_K [186], and it is well established—both theoretically and experimentally—that CP violation in D -meson mixing is extremely small. Consequently, any sizable CP-violating NP contribution could easily exceed the SM expectation.

Finally, for B_q -meson mixing, we can make use of SM predictions and compute both SM and NP contributions to meson mixing, using the approximation

$$\Delta m_{B_q} \simeq 2 \left| M_{12}^{\text{SM},q} + M_{12}^{\text{NP},q} \right|, \quad (\text{A16})$$

$$\phi_q = \arg \left(M_{12}^{\text{SM},q} + M_{12}^{\text{NP},q} \right). \quad (\text{A17})$$

The phases can be extracted from time-dependent asymmetries in B -meson decays, such as $B_s \rightarrow J/\psi \phi$ and $B \rightarrow J/\psi K_S$, yielding ϕ_s and ϕ_d , respectively. Other decay modes can also be used to determine these phases; in our analysis, we adopt the averages provided by HFLAV [187]. We note that possible penguin pollution effects are neglected in this work.

For $b \rightarrow s\gamma$ we used Flavio [188] to extract the bounds on the Wilson Coefficient. However, as we can see in Fig. 6, these bounds do not provide a competitive probe for the masses considered in the relic density computation.

Other significant $\Delta F = 1$ operators include the semileptonic operators, such as \mathcal{O}_{qe} and $\mathcal{O}_{q\ell}^{(1,3)}$, which contribute to well-measured meson decays like $B_s \rightarrow \mu\mu$ and $K \rightarrow \mu\mu$. However, to evaluate the contributions from these operators, one must work within the Low Energy EFT (LEFT) by integrating out the electroweak degrees of freedom. In this basis, the operators relevant to these processes are identified as \mathcal{O}_9 and \mathcal{O}_{10} , corresponding to the following vector and axial-vector operators:

$$\mathcal{O}_9 = \frac{4G_F}{\sqrt{2}} \frac{e^2}{(4\pi)^2} V_{tq} V_{tq'}^* [\bar{q}' \gamma_\mu P_L q] [\bar{\ell} \gamma^\mu \ell], \quad \mathcal{O}_{10} = \frac{4G_F}{\sqrt{2}} \frac{e^2}{(4\pi)^2} V_{tq} V_{tq'}^* [\bar{q}' \gamma_\mu P_L q] [\bar{\ell} \gamma^\mu \gamma_5 \ell]. \quad (\text{A18})$$

The matching from the SMEFT to these operators can be obtained using [189],

$$C_9 = \frac{4\pi^2}{e^2 V_{tq} V_{tq'}^* \Lambda^2} \frac{v^2}{\Lambda^2} \left[C_{qe} + C_{\ell q}^{(1)} + C_{\ell q}^{(3)} - (1 - 4s_W^2) (C_{Hq}^{(1)} + C_{Hq}^{(3)}) \right] = \frac{4\pi^2}{V_{tq} V_{tq'}^*} \frac{v^2}{M_\Phi^2} \frac{y_q^* y_{q'}}{432\pi^2} H(x_\Phi), \quad (\text{A19})$$

$$C_{10} = \frac{4\pi^2}{e^2 V_{tq} V_{tq'}^* \Lambda^2} \frac{v^2}{\Lambda^2} \left[C_{qe} - C_{\ell q}^{(1)} - C_{\ell q}^{(3)} + (C_{Hq}^{(1)} + C_{Hq}^{(3)}) \right] = 0, \quad (\text{A20})$$

and upon substituting the expressions for our model, we find that C_{10} vanishes exactly. Furthermore, this cancellation occurs within independent sets of operators: the singlet combination $C_{qe} - C_{\ell q}^{(1)} + C_{Hq}^{(1)} = 0$ and the triplet combination $C_{Hq}^{(3)} - C_{\ell q}^{(3)}$ cancel independently. A similar effect was noted in Ref. [168], where the different contributions to C_{10} were found to be proportional to the hypercharge, i.e., $C_{10} \sim (Y_e - Y_\ell - Y_H) = 0$, vanishing due to the conservation of hypercharge in the Yukawa interactions $\bar{\ell} e H$. We observe the same phenomenon here; similarly to the leptophilic case, after integrating out the new heavy degrees of freedom, we obtain the redundant operator $\bar{q}' \gamma_\mu (\tau^i) q \partial_\nu B^{\mu\nu} (D_\nu W^{i,\mu\nu})$, where τ_i are the generators of $\text{SU}(2)_L$. When applying the equations of motion, the derivative acting on the field strength tensor is replaced by the conserved currents, e.g. $\partial_\nu B^{\mu\nu} = J_Y^\mu$. Consequently, all leptons couple proportionally to the hypercharge, explaining the cancellation in C_{10} , and analogously for the $\text{SU}(2)_L$ contribution.

The phenomenological consequence of this cancellation is that purely leptonic decays such as $B_s, K_L \rightarrow \mu\mu$ are insensitive to this type of NP. Therefore, we must rely on constraints from the C_9 operator, where $\Delta F = 1$ processes such as $B \rightarrow K^* \mu\mu$ provide the leading constraint. These observables currently exhibit experimental anomalies. Using Ref. [190], for $b \rightarrow s$ transitions we obtain:

$$\frac{M_\Phi}{\sqrt{|y_2^* y_3| H(x_\Phi)}} = 126 \pm 12 \text{ GeV}. \quad (\text{A21})$$

Such a low scale is already ruled out by other observables (see Section 4); hence, we do not consider this type of operator in our final analysis.

B. Flavour Reparametrization

As shown in Figs. 4, 5 the $\text{U}(1)^3$ limit is preserved by flavour observables. This is not the case in the quark sector, where analogous regions are ruled out by the misaligned flavour contributions to $D - \bar{D}$ or $K - \bar{K}$ mixing; see, for instance, Figs. 7, 8 near $\phi \sim 0, \pm\pi/2, \pm\pi$.

For the leptophilic case, it is therefore interesting to quantify how closely one must align to each of these points in order to satisfy the bounds. For this comparison, it is useful to note that the sphere in Fig. 2 can be parametrised with any of the three lepton flavours aligned at the north pole. This allows a visual comparison of the three different $\text{U}(1)^3$ points, since the north pole of the sphere plays a special role in this parametrisation.

In Fig. 11, we show the results for the reparametrisation for the Majorana case corresponding to the right-top plot in Fig. 4. We see that the bounds in terms of the angles $\theta_{\mu,e}$, which represent the angular deviation from the north pole, can be directly compared to θ_τ . This not only confirms that alignment to any of the three $\text{U}(1)^3$ directions is consistent with LFV observables, but also allows us to quantify the degree of alignment required. In fact, alignment to the third family is less constrained than alignment to the lighter families by approximately two orders of magnitude. This can be understood from the parametric suppression of lower-family observables such as $\mu \rightarrow e\gamma$, which scales as $\sin^4 \theta_\tau$ in the τ -basis, while in the electron and muon bases it behaves as $\sin^2 \theta_{\mu,e} \cos^2 \theta_{\mu,e}$. This shows that aligning to the τ direction leads to a faster decoupling of these observables than aligning to the other families.

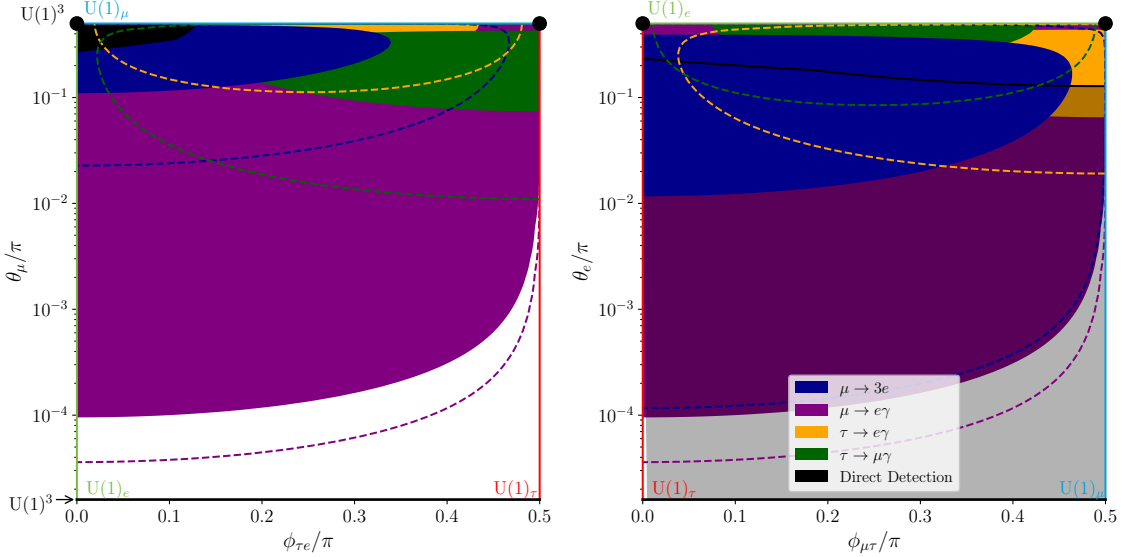


FIG. 11. Same bounds as in Fig. 4, but redefining the definition of the angles. In particular, the angle redefinition corresponds to aligning the μ - (e -)specific flavour to the north-pole of the sphere for the left (right) plot. In this case, we only consider the Majorana case with $\delta_{\text{DM}} = 0.14$ and $M_\chi = 170$ GeV.

C. Cross sections for dark matter freeze-out

Many of the cross sections employed in our analysis are taken from earlier studies, as detailed in the main text. In this Appendix, we collect only the cross sections that we have computed, including finite fermion mass effects for processes involving the Yukawa interaction. For completeness, we also present the corresponding expressions in the massless fermion limit. Throughout this section, we denote the SM fermion mass by m and expand the cross sections up to order v_{rel}^2 . Since the only relevant fermion mass is that of the top quark, the cross sections are computed either with a single massive fermion or with two massive fermions of equal mass in the final state. We do not provide expressions for the most general case of different fermion masses in the final state in order to avoid unnecessarily lengthy formulas. For the lepton case, one may simply put $N_c = 1$ in all expressions below.

The Majorana and Dirac DM pair annihilation into a massless fermion–antifermion pair reads, respectively,

$$\sigma_{\chi\chi}^{m=0} v_{\text{rel}} = \frac{y^4 N_c}{48\pi} \frac{M_\chi^2 (M_\chi^4 + M_\Phi^4)}{(M_\chi^2 + M_\Phi^2)^4} v_{\text{rel}}^2, \quad (\text{C1})$$

$$\sigma_{\chi\chi}^{m=0} v_{\text{rel}} = \frac{y^4 N_c}{32\pi} \frac{M_\chi^2}{(M_\chi^2 + M_\Phi^2)^2} \left(1 + \frac{(M_\Phi^4 - 3M_\Phi^2 M_\chi^2 - M_\chi^4)}{3(M_\chi^2 + M_\Phi^2)^2} v_{\text{rel}}^2 \right). \quad (\text{C2})$$

The corresponding cross sections for one massive quark in the final state read

$$\begin{aligned} \sigma_{\chi\chi}^m v_{\text{rel}} = & \frac{y^4 N_c}{256\pi} \frac{(4M_\chi^2 - m^2)}{M_\chi^4 (2(M_\chi^2 + M_\Phi^2) - m^2)^2} \left\{ m^2 (4M_\chi^2 - m^2) + \frac{v_{\text{rel}}^2}{3(2(M_\chi^2 + M_\Phi^2) - m^2)^2} [m^8 - 7m^6 (M_\Phi^2 + M_\chi^2) \right. \\ & \left. + m^4 (7M_\Phi^4 + 38M_\Phi^2 M_\chi^2 + 27M_\chi^4) - 4m^2 M_\chi^2 (5M_\Phi^4 + 22M_\Phi^2 M_\chi^2 + 13M_\chi^4) + 64M_\chi^4 (M_\Phi^4 + M_\chi^4)] \right\}, \end{aligned} \quad (\text{C3})$$

for Majorana DM, whereas for Dirac DM, one finds

$$\begin{aligned} \sigma_{\chi\chi}^m v_{\text{rel}} = & \frac{y^4 N_c}{512\pi} \frac{(4M_\chi^2 - m^2)}{M_\chi^4 (2(M_\chi^2 + M_\Phi^2) - m^2)^2} \left\{ 16M_\chi^4 - m^4 + \frac{v_{\text{rel}}^2}{3(2(M_\chi^2 + M_\Phi^2) - m^2)^2} [m^8 - m^6 (7M_\Phi^2 + 2M_\chi^2) \right. \\ & \left. + m^4 (7M_\Phi^4 + 14M_\Phi^2 M_\chi^2 - 9M_\chi^4) + 4m^2 M_\chi^2 (M_\Phi^4 + 2M_\Phi^2 M_\chi^2 + 17M_\chi^4) + 64M_\chi^4 (M_\Phi^4 - 3M_\chi^2 M_\Phi^2 + M_\chi^4)] \right\}. \end{aligned} \quad (\text{C4})$$

The cross sections for two massive quarks in the final state read, for Majorana and Dirac DM respectively, as follows

$$\begin{aligned} \sigma_{\chi\chi}^{2m} v_{\text{rel}} = & \frac{y^4 N_c}{32\pi} \frac{\sqrt{1 - m^2/M_\chi^2}}{(M_\Phi^2 + M_\Phi^2 - m^2)^2} \left\{ m^2 + \frac{v_{\text{rel}}^2}{24(M_\Phi^2 + M_\Phi^2 - m^2)^2 (M_\chi^2 - m^2)} [13m^8 - 2m^6 (13M_\Phi^2 + 18M_\chi^2) \right. \\ & \left. + m^4 (13M_\Phi^4 + 70M_\Phi^2 M_\chi^2 + 49M_\chi^4) - 2m^2 M_\chi^2 (13M_\Phi^4 + 22M_\Phi^2 M_\chi^2 + 21M_\chi^4) + 16M_\chi^4 (M_\Phi^4 + M_\chi^4)] \right\}, \end{aligned} \quad (\text{C5})$$

$$\sigma_{\chi\bar{\chi}}^{2m} v_{\text{rel}} = \frac{y^4 N_c}{32\pi} \frac{\sqrt{1-m^2/M_\chi^2}}{(M_\Phi^2 + M_\Phi^2 - m^2)^2} \left\{ M_\chi^2 + \frac{v_{\text{rel}}^2}{24(M_\Phi^2 + M_\Phi^2 - m^2)^2(M_\chi^2 - m^2)} [2m^8 - m^6(4M_\Phi^2 - 5M_\chi^2) + 2m^4(M_\Phi^4 + M_\Phi^2 M_\chi^2 - 12M_\chi^4) - m^2 M_\chi^2(7M_\Phi^4 - 26M_\Phi^2 M_\chi^2 - 25M_\chi^4) + 8M_\chi^4(M_\Phi^4 - 3M_\Phi^2 M_\chi^2 - M_\chi^4)] \right\}. \quad (\text{C6})$$

The cross sections with a finite fermion mass in Eqs. (C3)-(C6) reproduce the ones given in Eqs. (C1) and (C2) for $m \rightarrow 0$.

Only in the case of Majorana dark matter a Yukawa-driven annihilation channel for the mediator into two fermions exist, namely $\Phi\Phi \rightarrow e_i e_j$ and $\Phi\Phi \rightarrow q_i q_j$, together with their complex-conjugate processes, for the leptophilic and quarkphilic scenarios, respectively. As in the case of dark matter annihilations, only interactions involving quarks induce a flavour dependence in the total cross section. In the following, we therefore list the relevant cross sections with one massive quark and with two massive quarks in the final state, and provide the massless limit as a reference. The expressions read as follows

$$\sigma_{\Phi\Phi}^{m=0} v_{\text{rel}} = \frac{y^4 M_\chi^2}{6\pi(M_\chi^2 + M_\Phi^2)^2} \left[1 - \frac{M_\Phi^2(6M_\chi^2 + M_\Phi^2)}{6(M_\chi^2 + M_\Phi^2)^2} v_{\text{rel}}^2 \right], \quad (\text{C7})$$

$$\begin{aligned} \sigma_{\Phi\Phi}^m v_{\text{rel}} = & \frac{y^4 M_\chi^2(4M_\Phi^2 - m^2)}{768\pi M_\Phi^4(M_\chi^2 + M_\Phi^2)^2(M_\Phi^2 + M_\chi^2 - m^2)^2} \left\{ [8(M_\Phi^2 + M_\chi^2)^2 - 8m^2(M_\chi^2 + M_\Phi^2) + 3m^4](4M_\Phi^2 - m^2) \right. \\ & - \frac{v_{\text{rel}}^2}{48(M_\Phi^2 + M_\Phi^2 - m^2)^2(M_\chi^2 + M_\Phi^2)^2} [9m^{14} - 2m^{12}(19M_\chi^2 + 73M_\Phi^2) + 2m^{10}(142M_\chi^2 M_\Phi^2 + 365M_\Phi^4 - 7M_\chi^4) \\ & - 8m^8(200M_\Phi^6 + 63M_\Phi^4 M_\chi^2 - 102M_\Phi^2 M_\chi^4 - 37M_\chi^6) \\ & + 4m^6(379M_\Phi^8 - 308M_\Phi^6 M_\chi^2 - 1302M_\Phi^4 M_\chi^4 - 772M_\Phi^2 M_\chi^6 - 157M_\chi^8) \\ & - 16m^4(M_\Phi^2 + M_\chi^2)^2(7M_\Phi^6 - 342M_\chi^2 M_\Phi^4 - 153M_\chi^4 M_\Phi^2 - 36M_\chi^6) \\ & \left. - 64m^2(M_\Phi^2 + M_\chi^2)^3(3M_\chi^6 + 14M_\Phi^6 + 66M_\chi^2 M_\Phi^4 + 15M_\chi^4 M_\Phi^2) + 256M_\Phi^4(M_\chi^2 + M_\Phi^2)^4(6M_\chi^2 + M_\Phi^2) \right\}, \end{aligned} \quad (\text{C8})$$

$$\begin{aligned} \sigma_{\Phi\Phi}^{2m} v_{\text{rel}} = & \frac{y^4}{12\pi} \frac{M_\chi^2}{M_\Phi^3(M_\Phi^2 + M_\Phi^2 - m^2)^2 \sqrt{M_\Phi^2 - m^2}} \left\{ 2M_\Phi^4 - 3m^2 M_\Phi^2 + m^4 + \frac{v_{\text{rel}}^2}{24(M_\Phi^2 + M_\Phi^2 - m^2)^2} [3m^2 M_\chi^4(4M_\Phi^2 - 3m^2) \right. \\ & \left. - 6M_\chi^2(M_\Phi^2 - m^2)(3m^4 - 8m^2 M_\Phi^2 + 8M_\Phi^4) - (M_\Phi^2 - m^2)^2(9m^4 - 16m^2 M_\Phi^2 + 8M_\Phi^4)] \right\}. \end{aligned} \quad (\text{C9})$$

[1] P. Gondolo and G. Gelmini, *Cosmic abundances of stable particles: Improved analysis*, *Nucl. Phys. B* **360** (1991) 145–179.

[2] K. Griest and D. Seckel, *Three exceptions in the calculation of relic abundances*, *Phys. Rev. D* **43** (1991) 3191–3203.

[3] M. Cirelli, A. Strumia, and J. Zupan, *Dark Matter*, [arXiv:2406.01705](https://arxiv.org/abs/2406.01705).

[4] G. Arcadi, M. Dutra, P. Ghosh, M. Lindner, Y. Mambrini, M. Pierre, S. Profumo, and F. S. Queiroz, *The waning of the WIMP? A review of models, searches, and constraints*, *Eur. Phys. J. C* **78** (2018), no. 3 203, [arXiv:1703.07364](https://arxiv.org/abs/1703.07364).

[5] M. Schumann, *Direct Detection of WIMP Dark Matter: Concepts and Status*, *J. Phys. G* **46** (2019), no. 10 103003, [arXiv:1903.03026](https://arxiv.org/abs/1903.03026).

[6] G. Arcadi, D. Cabo-Almeida, M. Dutra, P. Ghosh, M. Lindner, Y. Mambrini, J. P. Neto, M. Pierre, S. Profumo, and F. S. Queiroz, *The Waning of the WIMP: Endgame?*, *Eur. Phys. J. C* **85** (2025), no. 2 152, [arXiv:2403.15860](https://arxiv.org/abs/2403.15860).

[7] M. Cirelli, N. Fornengo, and A. Strumia, *Minimal dark matter*, *Nucl. Phys. B* **753** (2006) 178–194, [hep-ph/0512090](https://arxiv.org/abs/hep-ph/0512090).

[8] S. Chang, R. Edezhath, J. Hutchinson, and M. Luty, *Effective WIMPs*, *Phys. Rev. D* **89** (2014), no. 1 015011, [arXiv:1307.8120](https://arxiv.org/abs/1307.8120).

[9] A. De Simone and T. Jacques, *Simplified models vs. effective field theory approaches in dark matter searches*, *Eur. Phys. J. C* **76** (2016), no. 7 367, [arXiv:1603.08002](https://arxiv.org/abs/1603.08002).

[10] C. Arina et al., *t-channel dark matter models – a whitepaper*, *Eur. Phys. J. C* **85** (2025) 975, [arXiv:2504.10597](https://arxiv.org/abs/2504.10597). [Erratum: Eur.Phys.J.C 85, 1105 (2025)].

[11] M. Garny, A. Ibarra, and S. Vogl, *Signatures of Majorana dark matter with t-channel mediators*, *Int. J. Mod. Phys. D* **24** (2015), no. 07 1530019, [arXiv:1503.01500](https://arxiv.org/abs/1503.01500).

[12] M. Garny, A. Ibarra, and S. Vogl, *Dark matter annihilations into two light fermions and one gauge boson: General analysis and antiproton constraints*, *JCAP* **04** (2012) 033, [arXiv:1112.5155](https://arxiv.org/abs/1112.5155).

[13] Y. Bai and J. Berger, *Fermion Portal Dark Matter*, *JHEP* **11** (2013) 171, [arXiv:1308.0612](https://arxiv.org/abs/1308.0612).

[14] A. DiFranzo, K. I. Nagao, A. Rajaraman, and T. M. P. Tait, *Simplified Models for Dark Matter Interacting with Quarks*, *JHEP* **11** (2013) 014, [arXiv:1308.2679](https://arxiv.org/abs/1308.2679). [Erratum: JHEP 01, 162 (2014)].

[15] H. An, L.-T. Wang, and H. Zhang, *Dark matter with t-channel mediator: a simple step beyond contact interaction*, *Phys. Rev. D* **89** (2014), no. 11 115014, [arXiv:1308.0592](https://arxiv.org/abs/1308.0592).

[16] M. Garny, A. Ibarra, S. Rydbeck, and S. Vogl, *Majorana Dark Matter with a Coloured Mediator: Collider vs Direct and Indirect Searches*, *JHEP* **06** (2014) 169, [arXiv:1403.4634](https://arxiv.org/abs/1403.4634).

[17] J. Kopp, L. Michaels, and J. Smirnov, *Loopy Constraints on Leptophilic Dark Matter and Internal Bremsstrahlung*, *JCAP* **04** (2014) 022, [[arXiv:1401.6457](#)].

[18] S. Biondini, L. Tiberi, and O. Panella, *Connecting t-channel dark matter models to the Standard Model Effective Field Theory*, *JHEP* **10** (2025) 060, [[arXiv:2507.00925](#)].

[19] M. R. Buckley, D. Feld, and D. Goncalves, *Scalar Simplified Models for Dark Matter*, *Phys. Rev. D* **91** (2015) 015017, [[arXiv:1410.6497](#)].

[20] J. Abdallah et al., *Simplified Models for Dark Matter Searches at the LHC*, *Phys. Dark Univ.* **9-10** (2015) 8–23, [[arXiv:1506.03116](#)].

[21] A. Boveia et al., *Recommendations on presenting LHC searches for missing transverse energy signals using simplified s-channel models of dark matter*, *Phys. Dark Univ.* **27** (2020) 100365, [[arXiv:1603.04156](#)].

[22] D. Goncalves, P. A. N. Machado, and J. M. No, *Simplified Models for Dark Matter Face their Consistent Completions*, *Phys. Rev. D* **95** (2017), no. 5 055027, [[arXiv:1611.04593](#)].

[23] A. Albert et al., *Towards the next generation of simplified Dark Matter models*, *Phys. Dark Univ.* **16** (2017) 49–70, [[arXiv:1607.06680](#)].

[24] N. F. Bell, G. Busoni, and I. W. Sanderson, *Self-consistent Dark Matter Simplified Models with an s-channel scalar mediator*, *JCAP* **03** (2017) 015, [[arXiv:1612.03475](#)].

[25] C. Englert, M. McCullough, and M. Spannowsky, *S-Channel Dark Matter Simplified Models and Unitarity*, *Phys. Dark Univ.* **14** (2016) 48–56, [[arXiv:1604.07975](#)].

[26] F. Kahlhoefer, K. Schmidt-Hoberg, T. Schwetz, and S. Vogl, *Implications of unitarity and gauge invariance for simplified dark matter models*, *JHEP* **02** (2016) 016, [[arXiv:1510.02110](#)].

[27] B. Belfatto, M. Blanke, J. Heisig, M. Krämer, L. Rathmann, and F. Wilsch, *Toward a Comprehensive Exploration of Flavored Dark Matter Models*, [arXiv:2511.10490](#).

[28] J. Kile and A. Soni, *Flavored Dark Matter in Direct Detection Experiments and at LHC*, *Phys. Rev. D* **84** (2011) 035016, [[arXiv:1104.5239](#)].

[29] J. F. Kamenik and J. Zupan, *Discovering Dark Matter Through Flavor Violation at the LHC*, *Phys. Rev. D* **84** (2011) 111502, [[arXiv:1107.0623](#)].

[30] P. Agrawal, S. Blanchet, Z. Chacko, and C. Kilic, *Flavored Dark Matter, and Its Implications for Direct Detection and Colliders*, *Phys. Rev. D* **86** (2012) 055002, [[arXiv:1109.3516](#)].

[31] P. Agrawal, Z. Chacko, E. C. F. S. Fortes, and C. Kilic, *Skew-Flavored Dark Matter*, *Phys. Rev. D* **93** (2016), no. 10 103510, [[arXiv:1511.06293](#)].

[32] M. Blanke, S. Das, and S. Kast, *Flavoured Dark Matter Moving Left*, *JHEP* **02** (2018) 105, [[arXiv:1711.10493](#)].

[33] G. Arcadi, L. Calibbi, M. Fedele, and F. Mescia, *Systematic approach to B-physics anomalies and t-channel dark matter*, *Phys. Rev. D* **104** (2021), no. 11 115012, [[arXiv:2103.09835](#)].

[34] H. Acaroğlu and M. Blanke, *Tasting flavoured Majorana dark matter*, *JHEP* **05** (2022) 086, [[arXiv:2109.10357](#)].

[35] G. Arcadi, L. Calibbi, M. Fedele, and F. Mescia, *Muon $g - 2$ and B-anomalies from Dark Matter*, *Phys. Rev. Lett.* **127** (2021), no. 6 061802, [[arXiv:2104.03228](#)].

[36] G. Demetriou, G. Isidori, G. Piazza, and E. Pilsard, *The third-generation-philic WIMP: an EFT analysis*, *Eur. Phys. J. C* **85** (2025), no. 8 865, [[arXiv:2505.04708](#)].

[37] W. Altmannshofer and A. Greljo, *Recent Progress in Flavor Model Building*, [arXiv:2412.04549](#).

[38] G. Isidori, *Flavour Physics and CP Violation*, [arXiv:2503.14042](#).

[39] Y. Nir, *Flavour physics and CP violation*, *CERN Yellow Rep. School Proc.* **5** (2020) 79–128.

[40] W. Altmannshofer and P. Stangl, *Flavour Physics Beyond the Standard Model*, [arXiv:2508.03950](#).

[41] J. de Blas et al., *Physics Briefing Book: Input for the 2026 update of the European Strategy for Particle Physics*, [arXiv:2511.03883](#).

[42] D. A. Faroughy, G. Isidori, F. Wilsch, and K. Yamamoto, *Flavour symmetries in the SMEFT*, *JHEP* **08** (2020) 166, [[arXiv:2005.05366](#)].

[43] A. Greljo, A. Palavrić, and A. E. Thomsen, *Adding Flavor to the SMEFT*, *JHEP* **10** (2022) 010, [[arXiv:2203.09561](#)].

[44] A. Greljo, A. Palavrić, and B. A. Stefanek, *Minimal Flavor Protection for TeV-scale New Physics*, [arXiv:2512.04159](#).

[45] F. Mescia, S. Okawa, and K. Wu, *Multi-component dark matter from Minimal Flavor Violation*, *JHEP* **11** (2024) 114, [[arXiv:2408.16812](#)].

[46] J. Kile, A. Kobach, and A. Soni, *Lepton-Flavored Dark Matter*, *Phys. Lett. B* **744** (2015) 330–338, [[arXiv:1411.1407](#)].

[47] G. D’Ambrosio, G. F. Giudice, G. Isidori, and A. Strumia, *Minimal flavor violation: An Effective field theory approach*, *Nucl. Phys. B* **645** (2002) 155–187, [[hep-ph/0207036](#)].

[48] B. Batell, J. Pradler, and M. Spannowsky, *Dark Matter from Minimal Flavor Violation*, *JHEP* **08** (2011) 038, [[arXiv:1105.1781](#)].

[49] L. Lopez-Honorez and L. Merlo, *Dark matter within the minimal flavour violation ansatz*, *Phys. Lett. B* **722** (2013) 135–143, [[arXiv:1303.1087](#)].

[50] P. Agrawal, B. Batell, D. Hooper, and T. Lin, *Flavored Dark Matter and the Galactic Center Gamma-Ray Excess*, *Phys. Rev. D* **90** (2014), no. 6 063512, [[arXiv:1404.1373](#)].

[51] P. Agrawal, M. Blanke, and K. Gemmeler, *Flavored Dark Matter beyond Minimal Flavor Violation*, *JHEP* **10** (2014) 072, [[arXiv:1405.6709](#)].

[52] M. Blanke and S. Kast, *Top-Flavoured Dark Matter in Dark Minimal Flavour Violation*, *JHEP* **05** (2017) 162, [[arXiv:1702.08457](#)].

[53] M.-C. Chen, J. Huang, and V. Takhistov, *Beyond Minimal Lepton Flavored Dark Matter*, *JHEP* **02** (2016) 060, [[arXiv:1510.04694](#)].

[54] H. Acaroğlu, P. Agrawal, and M. Blanke, *Lepton-flavoured scalar dark matter in Dark Minimal Flavour*

Violation, *JHEP* **05** (2023) 106, [[arXiv:2211.03809](#)].

[55] J. de Blas, J. C. Criado, M. Perez-Victoria, and J. Santiago, *Effective description of general extensions of the Standard Model: the complete tree-level dictionary*, *JHEP* **03** (2018) 109, [[arXiv:1711.10391](#)].

[56] A. Greljo and A. Palavrić, *Leading directions in the SMEFT*, *JHEP* **09** (2023) 009, [[arXiv:2305.08898](#)].

[57] A. Greljo, A. Palavrić, and A. Smolković, *Leading directions in the SMEFT: Renormalization effects*, *Phys. Rev. D* **109** (2024), no. 7 075033, [[arXiv:2312.09179](#)].

[58] V. Gherardi, D. Marzocca, M. Nardecchia, and A. Romanino, *Rank-One Flavor Violation and B-meson anomalies*, *JHEP* **10** (2019) 112, [[arXiv:1903.10954](#)].

[59] D. Marzocca, M. Nardecchia, A. Stanzione, and C. Toni, *Implications of $B \rightarrow K\nu\bar{\nu}$ under rank-one flavor violation hypothesis*, *Eur. Phys. J. C* **84** (2024), no. 11 1217, [[arXiv:2404.06533](#)].

[60] F. Bishara, A. Greljo, J. F. Kamenik, E. Stamou, and J. Zupan, *Dark Matter and Gauged Flavor Symmetries*, *JHEP* **12** (2015) 130, [[arXiv:1505.03862](#)].

[61] S. L. Glashow, J. Iliopoulos, and L. Maiani, *Weak Interactions with Lepton-Hadron Symmetry*, *Phys. Rev. D* **2** (1970) 1285–1292.

[62] A. Glioti, R. Rattazzi, L. Ricci, and L. Vecchi, *Exploring the flavor symmetry landscape*, *SciPost Phys.* **18** (2025), no. 6 201, [[arXiv:2402.09503](#)].

[63] R. S. Chivukula and H. Georgi, *Composite Technicolor Standard Model*, *Phys. Lett. B* **188** (1987) 99–104.

[64] A. Greljo and D. Marzocca, *High- p_T dilepton tails and flavor physics*, *Eur. Phys. J. C* **77** (2017), no. 8 548, [[arXiv:1704.09015](#)].

[65] L. Allwicher, D. A. Faroughy, F. Jaffredo, O. Sumensari, and F. Wilsch, *Drell-Yan tails beyond the Standard Model*, *JHEP* **03** (2023) 064, [[arXiv:2207.10714](#)].

[66] A. Greljo, J. Salko, A. Smolković, and P. Stangl, *Rare b decays meet high-mass Drell-Yan*, *JHEP* **05** (2023) 087, [[arXiv:2212.10497](#)].

[67] R. Barbieri, G. Isidori, J. Jones-Perez, P. Lodone, and D. M. Straub, *$U(2)$ and Minimal Flavour Violation in Supersymmetry*, *Eur. Phys. J. C* **71** (2011) 1725, [[arXiv:1105.2296](#)].

[68] R. Barbieri, D. Buttazzo, F. Sala, and D. M. Straub, *Flavour physics from an approximate $U(2)^3$ symmetry*, *JHEP* **07** (2012) 181, [[arXiv:1203.4218](#)].

[69] L. Allwicher, C. Cornellà, G. Isidori, and B. A. Stefanek, *New physics in the third generation. A comprehensive SMEFT analysis and future prospects*, *JHEP* **03** (2024) 049, [[arXiv:2311.00020](#)].

[70] J. Fuentes-Martín, G. Isidori, J. Pagès, and K. Yamamoto, *With or without $U(2)$? Probing non-standard flavor and helicity structures in semileptonic B decays*, *Phys. Lett. B* **800** (2020) 135080, [[arXiv:1909.02519](#)].

[71] M. J. Baker et al., *The Coannihilation Codex*, *JHEP* **12** (2015) 120, [[arXiv:1510.03434](#)].

[72] S. Biondini and M. Laine, *Thermal dark matter co-annihilating with a strongly interacting scalar*, *JHEP* **04** (2018) 072, [[arXiv:1801.05821](#)].

[73] M. Garny and J. Heisig, *Interplay of super-WIMP and freeze-in production of dark matter*, *Phys. Rev. D* **98** (2018), no. 9 095031, [[arXiv:1809.10135](#)].

[74] M. Becker, E. Copello, J. Harz, K. A. Mohan, and D. Sengupta, *Impact of Sommerfeld effect and bound state formation in simplified t -channel dark matter models*, *JHEP* **08** (2022) 145, [[arXiv:2203.04326](#)].

[75] S. Biondini and S. Vogl, *Coloured coannihilations: Dark matter phenomenology meets non-relativistic EFTs*, *JHEP* **02** (2019) 016, [[arXiv:1811.02581](#)].

[76] S. Biondini and S. Vogl, *Scalar dark matter coannihilating with a coloured fermion*, *JHEP* **11** (2019) 147, [[arXiv:1907.05766](#)].

[77] J. Bollig and S. Vogl, *Impact of bound states on non-thermal dark matter production*, *JCAP* **10** (2022) 031, [[arXiv:2112.01491](#)].

[78] J. Edsjo and P. Gondolo, *Neutralino relic density including coannihilations*, *Phys. Rev. D* **56** (1997) 1879–1894, [[hep-ph/9704361](#)].

[79] J. Ellis, K. A. Olive, and J. Zheng, *The Extent of the Stop Coannihilation Strip*, *Eur. Phys. J. C* **74** (2014) 2947, [[arXiv:1404.5571](#)].

[80] S. Biondini and M. Laine, *Re-derived overclosure bound for the inert doublet model*, *JHEP* **08** (2017) 047, [[arXiv:1706.01894](#)].

[81] Y.-L. S. Tsai, C.-T. Lu, and V. Q. Tran, *Confronting dark matter co-annihilation of Inert two Higgs Doublet Model with a compressed mass spectrum*, *JHEP* **06** (2020) 033, [[arXiv:1912.08875](#)].

[82] S. Biondini, P. Schicho, and T. V. I. Tenkanen, *Strong electroweak phase transition in t -channel simplified dark matter models*, *JCAP* **10** (2022) 044, [[arXiv:2207.12207](#)].

[83] A. Ibarra, T. Toma, M. Totzauer, and S. Wild, *Sharp Gamma-ray Spectral Features from Scalar Dark Matter Annihilations*, *Phys. Rev. D* **90** (2014), no. 4 043526, [[arXiv:1405.6917](#)].

[84] J. Hisano, S. Matsumoto, M. M. Nojiri, and O. Saito, *Non-perturbative effect on dark matter annihilation and gamma ray signature from galactic center*, *Phys. Rev. D* **71** (2005) 063528, [[hep-ph/0412403](#)].

[85] R. Iengo, *Sommerfeld enhancement: General results from field theory diagrams*, *JHEP* **05** (2009) 024, [[arXiv:0902.0688](#)].

[86] J. L. Feng, M. Kaplinghat, and H.-B. Yu, *Sommerfeld Enhancements for Thermal Relic Dark Matter*, *Phys. Rev. D* **82** (2010) 083525, [[arXiv:1005.4678](#)].

[87] W. Detmold, M. McCullough, and A. Pochinsky, *Dark Nuclei I: Cosmology and Indirect Detection*, *Phys. Rev. D* **90** (2014), no. 11 115013, [[arXiv:1406.2276](#)].

[88] B. von Harling and K. Petraki, *Bound-state formation for thermal relic dark matter and unitarity*, *JCAP* **12** (2014) 033, [[arXiv:1407.7874](#)].

[89] K. Petraki, M. Postma, and M. Wiechers, *Dark-matter bound states from Feynman diagrams*, *JHEP* **06** (2015) 128, [[arXiv:1505.00109](#)].

[90] S. Biondini, M. Eriksson, and M. Laine, *Computing singlet scalar freeze-out with plasmon and plasmino states*,

JHEP **08** (2025) 197, [[arXiv:2505.05206](#)].

[91] J. Harz and K. Petraki, *Higgs-mediated bound states in dark-matter models*, *JHEP* **04** (2019) 130, [[arXiv:1901.10030](#)].

[92] P. Olgoso, P. Paradisi, and N. Selimovic, *The Dark Side of a Tera-Z Factory*, [arXiv:2507.17803](#).

[93] J. Liu, X.-P. Wang, and K.-P. Xie, *Searching for lepton portal dark matter with colliders and gravitational waves*, *JHEP* **06** (2021) 149, [[arXiv:2104.06421](#)].

[94] **Planck** Collaboration, N. Aghanim et al., *Planck 2018 results. VI. Cosmological parameters*, *Astron. Astrophys.* **641** (2020) A6, [[arXiv:1807.06209](#)]. [Erratum: *Astron. Astrophys.* 652, C4 (2021)].

[95] A. Ibarra and S. Wild, *Dirac dark matter with a charged mediator: a comprehensive one-loop analysis of the direct detection phenomenology*, *JCAP* **05** (2015) 047, [[arXiv:1503.03382](#)].

[96] J. Hisano, R. Nagai, and N. Nagata, *Singlet Dirac Fermion Dark Matter with Mediators at Loop*, *JHEP* **12** (2018) 059, [[arXiv:1808.06301](#)].

[97] G. Arcadi, D. Cabo-Almeida, F. Mescia, and J. Virto, *Dark Matter Direct Detection in t-channel mediator models*, *JCAP* **02** (2024) 005, [[arXiv:2309.07896](#)].

[98] A. Ibarra, M. Reichard, and G. Tomar, *Probing dark matter electromagnetic properties in direct detection experiments*, *JCAP* **02** (2025) 072, [[arXiv:2408.15760](#)].

[99] B. Kayser and A. S. Goldhaber, *CPT and CP Properties of Majorana Particles, and the Consequences*, *Phys. Rev. D* **28** (1983) 2341.

[100] E. E. Radescu, *Comments on the Electromagnetic Properties of Majorana Fermions*, *Phys. Rev. D* **32** (1985) 1266.

[101] J. Bramante, P. J. Fox, G. D. Kribs, and A. Martin, *Inelastic frontier: Discovering dark matter at high recoil energy*, *Phys. Rev. D* **94** (2016), no. 11 115026, [[arXiv:1608.02662](#)].

[102] **LZ** Collaboration, J. Aalbers et al., *Dark Matter Search Results from 4.2 Tonne-Years of Exposure of the LUX-ZEPLIN (LZ) Experiment*, *Phys. Rev. Lett.* **135** (2025), no. 1 011802, [[arXiv:2410.17036](#)].

[103] **DARWIN** Collaboration, J. Aalbers et al., *DARWIN: towards the ultimate dark matter detector*, *JCAP* **11** (2016) 017, [[arXiv:1606.07001](#)].

[104] M. Garny, J. Heisig, M. Hufnagel, and B. Lülf, *Top-philic dark matter within and beyond the WIMP paradigm*, *Phys. Rev. D* **97** (2018), no. 7 075002, [[arXiv:1802.00814](#)].

[105] M. Cirelli and G. Giesen, *Antiprotons from Dark Matter: Current constraints and future sensitivities*, *JCAP* **04** (2013) 015, [[arXiv:1301.7079](#)].

[106] S. El Hedri, A. Kaminska, and M. de Vries, *A Sommerfeld Toolbox for Colored Dark Sectors*, *Eur. Phys. J. C* **77** (2017), no. 9 622, [[arXiv:1612.02825](#)].

[107] P. De La Torre Luque, J. Smirnov, and T. Linden, *Gamma-ray lines in 15 years of Fermi-LAT data: New constraints on Higgs portal dark matter*, *Phys. Rev. D* **109** (2024), no. 4 L041301, [[arXiv:2309.03281](#)].

[108] T. Bringmann and C. Weniger, *Gamma Ray Signals from Dark Matter: Concepts, Status and Prospects*, *Phys. Dark Univ.* **1** (2012) 194–217, [[arXiv:1208.5481](#)].

[109] **Fermi-LAT** Collaboration, S. Abdollahi et al., *Incremental Fermi Large Area Telescope Fourth Source Catalog*, *Astrophys. J. Supp.* **260** (2022), no. 2 53, [[arXiv:2201.11184](#)].

[110] A. McDaniel, M. Ajello, C. M. Karwin, M. Di Mauro, A. Drlica-Wagner, and M. A. Sánchez-Conde, *Legacy analysis of dark matter annihilation from the Milky Way dwarf spheroidal galaxies with 14 years of Fermi-LAT data*, *Phys. Rev. D* **109** (2024), no. 6 063024, [[arXiv:2311.04982](#)].

[111] **HESS** Collaboration, H. Abdallah et al., *Search for γ -Ray Line Signals from Dark Matter Annihilations in the Inner Galactic Halo from 10 Years of Observations with H.E.S.S.*, *Phys. Rev. Lett.* **120** (2018), no. 20 201101, [[arXiv:1805.05741](#)].

[112] S. P. Martin, *A Supersymmetry primer*, *Adv. Ser. Direct. High Energy Phys.* **18** (1998) 1–98, [[hep-ph/9709356](#)].

[113] **ATLAS** Collaboration, G. Aad et al., *Search for electroweak production of charginos and sleptons decaying into final states with two leptons and missing transverse momentum in $\sqrt{s} = 13$ TeV pp collisions using the ATLAS detector*, *Eur. Phys. J. C* **80** (2020), no. 2 123, [[arXiv:1908.08215](#)].

[114] **ATLAS** Collaboration, G. Aad et al., *Searches for electroweak production of supersymmetric particles with compressed mass spectra in $\sqrt{s} = 13$ TeV pp collisions with the ATLAS detector*, *Phys. Rev. D* **101** (2020), no. 5 052005, [[arXiv:1911.12606](#)].

[115] **ATLAS** Collaboration, G. Aad et al., *Search for direct pair production of sleptons and charginos decaying to two leptons and neutralinos with mass splittings near the W-boson mass in $\sqrt{s} = 13$ TeV pp collisions with the ATLAS detector*, *JHEP* **06** (2023) 031, [[arXiv:2209.13935](#)].

[116] **CMS** Collaboration, V. Chekhovsky et al., *A general search for supersymmetric particles in scenarios with compressed mass spectra using proton-proton collisions at $\sqrt{s} = 13$ TeV*, [arXiv:2508.13900](#).

[117] **DELPHI** Collaboration, J. Abdallah et al., *Searches for supersymmetric particles in $e^+ e^-$ collisions up to 208-GeV and interpretation of the results within the MSSM*, *Eur. Phys. J. C* **31** (2003) 421–479, [[hep-ex/0311019](#)].

[118] **ATLAS** Collaboration, G. Aad et al., *Search for electroweak production of supersymmetric particles in final states with two τ -leptons in $\sqrt{s} = 13$ TeV pp collisions with the ATLAS detector*, *JHEP* **05** (2024) 150, [[arXiv:2402.00603](#)].

[119] **CMS** Collaboration, A. M. Sirunyan et al., *Search for Supersymmetry with a Compressed Mass Spectrum in Events with a Soft τ Lepton, a Highly Energetic Jet, and Large Missing Transverse Momentum in Proton-Proton Collisions at $\sqrt{s} = 13$ TeV*, *Phys. Rev. Lett.* **124** (2020), no. 4 041803, [[arXiv:1910.01185](#)].

[120] **OPAL** Collaboration, G. Abbiendi et al., *Search for nearly mass degenerate charginos and neutralinos at LEP*, *Eur. Phys. J. C* **29** (2003) 479–489, [[hep-ex/0210043](#)].

[121] L. Calibbi and G. Signorelli, *Charged Lepton Flavour Violation: An Experimental and Theoretical Introduction*, *Riv. Nuovo Cim.* **41** (2018), no. 2 71–174, [[arXiv:1709.00294](#)].

[122] L. Calibbi, T. Li, X. Marcano, and M. A. Schmidt, *Indirect constraints on lepton-flavor-violating quarkonium decays*, *Phys. Rev. D* **106** (2022), no. 11 115039, [[arXiv:2207.10913](https://arxiv.org/abs/2207.10913)].

[123] E. Fernández-Martínez, X. Marcano, and D. Naredo-Tuero, *Global lepton flavour violating constraints on new physics*, *Eur. Phys. J. C* **84** (2024), no. 7 666, [[arXiv:2403.09772](https://arxiv.org/abs/2403.09772)].

[124] A. Greljo, A. Palavrić, M. Tunja, and J. Zupan, *Expanding the Landscape of Exotic Muon Decays*, [[arXiv:2510.08674](https://arxiv.org/abs/2510.08674)].

[125] **MEG II** Collaboration, K. Afanaciev et al., *New limit on the $\mu^+ \rightarrow e^+ \gamma$ decay with the MEG II experiment*, *Eur. Phys. J. C* **85** (2025), no. 10 1177, [[arXiv:2504.15711](https://arxiv.org/abs/2504.15711)]. [Erratum: *Eur.Phys.J.C* 85, 1317 (2025)].

[126] **Mu2e** Collaboration, R. H. Bernstein, *The Mu2e Experiment*, *Front. in Phys.* **7** (2019) 1, [[arXiv:1901.11099](https://arxiv.org/abs/1901.11099)].

[127] **COMET** Collaboration, M. Moritsu, *Search for Muon-to-Electron Conversion with the COMET Experiment*, *†, Universe* **8** (2022), no. 4 196, [[arXiv:2203.06365](https://arxiv.org/abs/2203.06365)].

[128] A. Blondel et al., *Research Proposal for an Experiment to Search for the Decay $\mu \rightarrow eee$* , [[arXiv:1301.6113](https://arxiv.org/abs/1301.6113)].

[129] **Belle-II** Collaboration, W. Altmannshofer et al., *The Belle II Physics Book*, *PTEP* **2019** (2019), no. 12 123C01, [[arXiv:1808.10567](https://arxiv.org/abs/1808.10567)]. [Erratum: *PTEP* 2020, 029201 (2020)].

[130] M. Achasov et al., *STCF conceptual design report (Volume 1): Physics & detector*, *Front. Phys. (Beijing)* **19** (2024), no. 1 14701, [[arXiv:2303.15790](https://arxiv.org/abs/2303.15790)].

[131] **FCC** Collaboration, M. Benedikt et al., *Future Circular Collider Feasibility Study Report: Volume 1, Physics, Experiments, Detectors*, [[arXiv:2505.00272](https://arxiv.org/abs/2505.00272)].

[132] **MEG II** Collaboration, K. Afanaciev et al., *A search for $\mu^+ \rightarrow e^+ \gamma$ with the first dataset of the MEG II experiment*, *Eur. Phys. J. C* **84** (2024), no. 3 216, [[arXiv:2310.12614](https://arxiv.org/abs/2310.12614)]. [Erratum: *Eur.Phys.J.C* 84, 1042 (2024)].

[133] **BaBar** Collaboration, B. Aubert et al., *Searches for Lepton Flavor Violation in the Decays $\tau^\pm \rightarrow e^\pm \gamma$ and $\tau^\pm \rightarrow \mu^\pm \gamma$* , *Phys. Rev. Lett.* **104** (2010) 021802, [[arXiv:0908.2381](https://arxiv.org/abs/0908.2381)].

[134] **Belle** Collaboration, A. Abdesselam et al., *Search for lepton-flavor-violating tau-lepton decays to $\ell\gamma$ at Belle*, *JHEP* **10** (2021) 19, [[arXiv:2103.12994](https://arxiv.org/abs/2103.12994)].

[135] **COMET** Collaboration, R. Abramishvili et al., *COMET Phase-I Technical Design Report*, *PTEP* **2020** (2020), no. 3 033C01, [[arXiv:1812.09018](https://arxiv.org/abs/1812.09018)].

[136] **Mu2e** Collaboration, L. Bartoszek et al., *Mu2e Technical Design Report*, [[arXiv:1501.05241](https://arxiv.org/abs/1501.05241)].

[137] M. Cahill-Rowley, S. El Hedri, W. Shepherd, and D. G. E. Walker, *Perturbative Unitarity Constraints on Charged/Colored Portals*, *Phys. Dark Univ.* **22** (2018) 48–59, [[arXiv:1501.03153](https://arxiv.org/abs/1501.03153)].

[138] M. Garny, J. Heisig, B. Lülf, and S. Vogl, *Coannihilation without chemical equilibrium*, *Phys. Rev. D* **96** (2017), no. 10 103521, [[arXiv:1705.09292](https://arxiv.org/abs/1705.09292)].

[139] R. T. D’Agnolo, D. Pappadopulo, and J. T. Ruderman, *Fourth Exception in the Calculation of Relic Abundances*, *Phys. Rev. Lett.* **119** (2017), no. 6 061102, [[arXiv:1705.08450](https://arxiv.org/abs/1705.08450)].

[140] S. Banerjee et al., *Snowmass 2021 White Paper: Charged lepton flavor violation in the tau sector*, [[arXiv:2203.14919](https://arxiv.org/abs/2203.14919)].

[141] **MEG II** Collaboration, A. M. Baldini et al., *The design of the MEG II experiment*, *Eur. Phys. J. C* **78** (2018), no. 5 380, [[arXiv:1801.04688](https://arxiv.org/abs/1801.04688)].

[142] A. Ibarra, A. Pierce, N. R. Shah, and S. Vogl, *Anatomy of Coannihilation with a Scalar Top Partner*, *Phys. Rev. D* **91** (2015), no. 9 095018, [[arXiv:1501.03164](https://arxiv.org/abs/1501.03164)].

[143] A. De Simone, G. F. Giudice, and A. Strumia, *Benchmarks for Dark Matter Searches at the LHC*, *JHEP* **06** (2014) 081, [[arXiv:1402.6287](https://arxiv.org/abs/1402.6287)].

[144] S. El Hedri, A. Kaminska, M. de Vries, and J. Zurita, *Simplified Phenomenology for Colored Dark Sectors*, *JHEP* **04** (2017) 118, [[arXiv:1703.00452](https://arxiv.org/abs/1703.00452)].

[145] T. Binder, M. Garny, J. Heisig, S. Lederer, and K. Urban, *Excited bound states and their role in dark matter production*, *Phys. Rev. D* **108** (2023), no. 9 095030, [[arXiv:2308.01336](https://arxiv.org/abs/2308.01336)].

[146] M. Garny and J. Heisig, *Bound-state effects on dark matter coannihilation: Pushing the boundaries of conversion-driven freeze-out*, *Phys. Rev. D* **105** (2022), no. 5 055004, [[arXiv:2112.01499](https://arxiv.org/abs/2112.01499)].

[147] G. T. Bodwin, E. Braaten, and G. P. Lepage, *Rigorous QCD analysis of inclusive annihilation and production of heavy quarkonium*, *Phys. Rev. D* **51** (1995) 1125–1171, [[hep-ph/9407339](https://arxiv.org/abs/hep-ph/9407339)]. [Erratum: *Phys.Rev.D* 55, 5853 (1997)].

[148] A. Vairo, *A Theoretical review of heavy quarkonium inclusive decays*, *Mod. Phys. Lett. A* **19** (2004) 253–269, [[hep-ph/0311303](https://arxiv.org/abs/hep-ph/0311303)].

[149] A. Mitridate, M. Redi, J. Smirnov, and A. Strumia, *Cosmological Implications of Dark Matter Bound States*, *JCAP* **05** (2017) 006, [[arXiv:1702.01141](https://arxiv.org/abs/1702.01141)].

[150] J. Harz and K. Petraki, *Radiative bound-state formation in unbroken perturbative non-Abelian theories and implications for dark matter*, *JHEP* **07** (2018) 096, [[arXiv:1805.01200](https://arxiv.org/abs/1805.01200)].

[151] S. Biondini, N. Brambilla, G. Qerimi, and A. Vairo, *Effective field theories for dark matter pairs in the early universe: cross sections and widths*, *JHEP* **07** (2023) 006, [[arXiv:2304.00113](https://arxiv.org/abs/2304.00113)].

[152] T. Binder, K. Mukaida, and K. Petraki, *Rapid bound-state formation of Dark Matter in the Early Universe*, *Phys. Rev. Lett.* **124** (2020), no. 16 161102, [[arXiv:1910.11288](https://arxiv.org/abs/1910.11288)].

[153] S. Biondini, N. Brambilla, A. Dashko, G. Qerimi, and A. Vairo, *Effective field theories for dark matter pairs in the early universe: Debye mass effects*, *JHEP* **04** (2025) 091, [[arXiv:2501.03327](https://arxiv.org/abs/2501.03327)].

[154] T. Binder, A. Filimonova, K. Petraki, and G. White, *Saha equilibrium for metastable bound states and dark matter freeze-out*, *Phys. Lett. B* **833** (2022) 137323, [[arXiv:2112.00042](https://arxiv.org/abs/2112.00042)].

[155] M. Becker, E. Copello, J. Harz, and M. Napetschnig, *Manual for SE+BSF4DM – A micrOMEGAs package for Sommerfeld Effect and Bound State Formation in colored Dark Sectors*, [[arXiv:2512.02155](https://arxiv.org/abs/2512.02155)].

[156] **ATLAS** Collaboration, G. Aad et al., *The quest to discover supersymmetry at the ATLAS experiment*, *Phys. Rept.* **1116** (2025) 261–300, [[arXiv:2403.02455](https://arxiv.org/abs/2403.02455)].

[157] **ATLAS** Collaboration, M. Aaboud et al., *Search for dark matter and other new phenomena in events with an*

energetic jet and large missing transverse momentum using the ATLAS detector, *JHEP* **01** (2018) 126, [[arXiv:1711.03301](https://arxiv.org/abs/1711.03301)].

[158] CMS Collaboration, A. M. Sirunyan et al., *Searches for physics beyond the standard model with the M_{T2} variable in hadronic final states with and without disappearing tracks in proton-proton collisions at $\sqrt{s} = 13$ TeV*, *Eur. Phys. J. C* **80** (2020), no. 1 3, [[arXiv:1909.03460](https://arxiv.org/abs/1909.03460)].

[159] CMS Collaboration, T. C. Collaboration et al., *Search for supersymmetry in proton-proton collisions at 13 TeV in final states with jets and missing transverse momentum*, *JHEP* **10** (2019) 244, [[arXiv:1908.04722](https://arxiv.org/abs/1908.04722)].

[160] ATLAS Collaboration, G. Aad et al., *Search for squarks and gluinos in final states with jets and missing transverse momentum using 139 fb^{-1} of $\sqrt{s} = 13$ TeV pp collision data with the ATLAS detector*, *JHEP* **02** (2021) 143, [[arXiv:2010.14293](https://arxiv.org/abs/2010.14293)].

[161] ATLAS Collaboration, G. Aad et al., *Search for new phenomena in events with an energetic jet and missing transverse momentum in pp collisions at $\sqrt{s} = 13$ TeV with the ATLAS detector*, *Phys. Rev. D* **103** (2021), no. 11 112006, [[arXiv:2102.10874](https://arxiv.org/abs/2102.10874)].

[162] ATLAS Collaboration, G. Aad et al., *Search for a scalar partner of the top quark in the all-hadronic $t\bar{t}$ plus missing transverse momentum final state at $\sqrt{s} = 13$ TeV with the ATLAS detector*, *Eur. Phys. J. C* **80** (2020), no. 8 737, [[arXiv:2004.14060](https://arxiv.org/abs/2004.14060)].

[163] ATLAS Collaboration, G. Aad et al., *Search for new phenomena with top quark pairs in final states with one lepton, jets, and missing transverse momentum in pp collisions at $\sqrt{s} = 13$ TeV with the ATLAS detector*, *JHEP* **04** (2021) 174, [[arXiv:2012.03799](https://arxiv.org/abs/2012.03799)].

[164] ATLAS Collaboration, G. Aad et al., *Search for new phenomena with top-quark pairs and large missing transverse momentum using 140 fb^{-1} of pp collision data at $\sqrt{s} = 13$ TeV with the ATLAS detector*, *JHEP* **03** (2024) 139, [[arXiv:2401.13430](https://arxiv.org/abs/2401.13430)].

[165] ATLAS Collaboration, G. Aad et al., *Search for new phenomena in final states with b-jets and missing transverse momentum in $\sqrt{s} = 13$ TeV pp collisions with the ATLAS detector*, *JHEP* **05** (2021) 093, [[arXiv:2101.12527](https://arxiv.org/abs/2101.12527)].

[166] I. Doršner and A. Greljo, *Leptoquark toolbox for precision collider studies*, *JHEP* **05** (2018) 126, [[arXiv:1801.07641](https://arxiv.org/abs/1801.07641)].

[167] P. Gondolo and S. Scopel, *On the sbottom resonance in dark matter scattering*, *JCAP* **10** (2013) 032, [[arXiv:1307.4481](https://arxiv.org/abs/1307.4481)].

[168] J. Davighi and B. A. Stefanek, *Deconstructed hypercharge: a natural model of flavour*, *JHEP* **11** (2023) 100, [[arXiv:2305.16280](https://arxiv.org/abs/2305.16280)].

[169] R. Alarcon et al., *Electric dipole moments and the search for new physics*, in *Snowmass 2021*, 3, 2022, [[arXiv:2203.08103](https://arxiv.org/abs/2203.08103)].

[170] n2EDM Collaboration, N. J. Ayres et al., *The design of the n2EDM experiment: nEDM Collaboration*, *Eur. Phys. J. C* **81** (2021), no. 6 512, [[arXiv:2101.08730](https://arxiv.org/abs/2101.08730)].

[171] pEDM Collaboration, J. Alexander et al., *The storage ring proton EDM experiment*, [[arXiv:2205.00830](https://arxiv.org/abs/2205.00830)].

[172] J. R. Gaunt and A. Owen, *FeynCraft: A Game of Feynman Diagrams*, [[arXiv:2510.14082](https://arxiv.org/abs/2510.14082)].

[173] J. Fuentes-Martín, M. König, J. Pagès, A. E. Thomsen, and F. Wilsch, *A proof of concept for matchete: an automated tool for matching effective theories*, *Eur. Phys. J. C* **83** (2023), no. 7 662, [[arXiv:2212.04510](https://arxiv.org/abs/2212.04510)].

[174] L. Calibbi, X. Marcano, and J. Roy, *Z lepton flavour violation as a probe for new physics at future e^+e^- colliders*, *Eur. Phys. J. C* **81** (2021), no. 12 1054, [[arXiv:2107.10273](https://arxiv.org/abs/2107.10273)].

[175] Particle Data Group Collaboration, S. Navas et al., *Review of particle physics*, *Phys. Rev. D* **110** (2024), no. 3 030001.

[176] A. J. Buras and P. Stangl, *On the interplay of constraints from B_s, D , and K meson mixing in Z' models with implications for $b \rightarrow s \nu \bar{\nu}$ transitions*, *Eur. Phys. J. C* **85** (2025), no. 5 519, [[arXiv:2412.14254](https://arxiv.org/abs/2412.14254)].

[177] M. Gorbahn, S. Jäger, and S. Kvedaraitė, *RI-(S)MOM to \overline{MS} conversion for B_K at two-loop order*, *JHEP* **09** (2025) 011, [[arXiv:2411.19861](https://arxiv.org/abs/2411.19861)].

[178] R. J. Dowdall, C. T. H. Davies, R. R. Horgan, G. P. Lepage, C. J. Monahan, J. Shigemitsu, and M. Wingate, *Neutral B-meson mixing from full lattice QCD at the physical point*, *Phys. Rev. D* **100** (2019), no. 9 094508, [[arXiv:1907.01025](https://arxiv.org/abs/1907.01025)].

[179] L. Di Luzio, A. W. M. Guerrera, X. P. Díaz, and S. Rigolin, *On the IR/UV flavour connection in non-universal axion models*, *JHEP* **06** (2023) 046, [[arXiv:2304.04643](https://arxiv.org/abs/2304.04643)].

[180] M. Ciuchini et al., *Delta $M(K)$ and $\epsilon(K)$ in SUSY at the next-to-leading order*, *JHEP* **10** (1998) 008, [[hep-ph/9808328](https://arxiv.org/abs/hep-ph/9808328)].

[181] D. Becirevic, M. Ciuchini, E. Franco, V. Gimenez, G. Martinelli, A. Masiero, M. Papinutto, J. Reyes, and L. Silvestrini, *$B_d - \bar{B}_d$ mixing and the $B_d \rightarrow J/\psi K_s$ asymmetry in general SUSY models*, *Nucl. Phys. B* **634** (2002) 105–119, [[hep-ph/0112303](https://arxiv.org/abs/hep-ph/0112303)].

[182] UTfit Collaboration, M. Bona et al., *Model-independent constraints on $\Delta F = 2$ operators and the scale of new physics*, *JHEP* **03** (2008) 049, [[arXiv:0707.0636](https://arxiv.org/abs/0707.0636)].

[183] N. Carrasco et al., *$D^0 - \bar{D}^0$ mixing in the standard model and beyond from $N_f = 2$ twisted mass QCD*, *Phys. Rev. D* **90** (2014), no. 1 014502, [[arXiv:1403.7302](https://arxiv.org/abs/1403.7302)].

[184] Flavour Lattice Averaging Group (FLAG) Collaboration, Y. Aoki et al., *FLAG Review 2024*, [[arXiv:2411.04268](https://arxiv.org/abs/2411.04268)].

[185] J. Brod and M. Gorbahn, *Next-to-Next-to-Leading-Order Charm-Quark Contribution to the CP Violation Parameter ϵ_K and ΔM_K* , *Phys. Rev. Lett.* **108** (2012) 121801, [[arXiv:1108.2036](https://arxiv.org/abs/1108.2036)].

[186] J. Brod, M. Gorbahn, and E. Stamou, *Standard-Model Prediction of ϵ_K with Manifest Quark-Mixing Unitarity*, *Phys. Rev. Lett.* **125** (2020), no. 17 171803, [[arXiv:1911.06822](https://arxiv.org/abs/1911.06822)].

[187] Heavy Flavor Averaging Group (HFLAV) Collaboration, S. Banerjee et al., *Averages of b -hadron, c -hadron, and τ -lepton properties as of 2023*, [[arXiv:2411.18639](https://arxiv.org/abs/2411.18639)].

[188] D. M. Straub, *flavio: a Python package for flavour and precision phenomenology in the Standard Model and*

beyond, [arXiv:1810.08132](https://arxiv.org/abs/1810.08132).

- [189] R. Alonso, B. Grinstein, and J. Martin Camalich, *$SU(2) \times U(1)$ gauge invariance and the shape of new physics in rare B decays*, *Phys. Rev. Lett.* **113** (2014) 241802, [[arXiv:1407.7044](https://arxiv.org/abs/1407.7044)].
- [190] A. Greljo, H. Tiblom, and A. Valenti, *New physics through flavor tagging at FCC-ee*, *SciPost Phys.* **18** (2025), no. 5 152, [[arXiv:2411.02485](https://arxiv.org/abs/2411.02485)].